Open charm and charmonium production at relativistic energies

E. L. Bratkovskaya[1*], W. Cassing[2] and H. Stöcker[1]

[1] Institut für Theoretische Physik, Universität Frankfurt

60054 Frankfurt, Germany

[2] Institut für Theoretische Physik, Universität Giessen

35392 Giessen, Germany

Abstract

We calculate open charm and charmonium production in $Au + Au$ reactions at $\sqrt{s} = 200$ GeV within the hadron-string dynamics (HSD) transport approach employing open charm cross sections from pN and πN reactions that are fitted to results from PYTHIA and scaled in magnitude to the available experimental data. Charmonium dissociation with nucleons and formed mesons to open charm ($D + \bar{D}$ pairs) is included dynamically. The 'comover' dissociation cross sections are described by a simple phase-space model including a single free parameter, i.e. an interaction strength M_0^2, that is fitted to the J/Ψ suppression data for $Pb + Pb$ collisions at SPS energies. As a novel feature we implement the backward channels for charmonium reproduction by $D\bar{D}$ channels employing detailed balance. From our dynamical calculations we find that the charmonium recreation is comparable to the dissociation by 'comoving' mesons. This leads to the final result that the total J/Ψ suppression at $\sqrt{s} = 200$ GeV as a function of centrality is slightly less than the suppression seen at SPS energies by the NA50 Collaboration, where the 'comover' dissociation is substantial and

*Supported by DFG

the backward channels play no role. Furthermore, even in case that all directly produced J/Ψ mesons dissociate immediately (or are not formed as a mesonic state), a sizeable amount of charmonia is found asymptotically due to the $D + \bar{D} \rightarrow J/\Psi$ + meson channels in central collisions of $Au + Au$ at $\sqrt{s} = 200$ GeV which, however, is lower than the J/Ψ yield expected from binary scaling of pp collisions.

PACS: 25.75.-q; 13.60.Le; 14.40.Lb; 14.65.Dw

Keywords: Relativistic heavy-ion collisions; Meson production; Charmed mesons; Charmed quarks

I. INTRODUCTION

The dynamics of ultra-relativistic nucleus-nucleus collisions at SPS and RHIC energies are of fundamental interest with respect to the properties of hadronic/partonic systems at high energy densities as encountered in the early phase of the 'big bang'. Especially the formation of a quark-gluon plasma (QGP) and its transition to interacting hadronic matter has motivated a large community for about 20 to 30 years by now [1]. However, even after more than a decade of experiments at the Super Proton Synchrotron (SPS) and recently at the Relativistic Heavy-Ion Collider (RHIC) the complexity of the dynamics has not been unraveled and no conclusive evidence has been obtained for the formation of the QGP and/or the properties of the phase transition [2,3] though 'circumstantial evidence' has been claimed [4].

Apart from the light and strange flavor ($u, \bar{u}, d, \bar{d}, s, \bar{s}$) quark physics and their hadronic bound states in the vacuum (π, K, ϕ etc.) the interest in hadronic states with charm flavors ($c, \bar{c}$) has been rising additionally in line with the development of new experimental facilities. This relates to the charm production cross section in pN, πN, pA and AA reactions as well as to their interactions with baryons and mesons which determine their properties (spectral functions) in the hadronic medium.

The charm quark degrees of freedom are of special interest in context with the phase transition to the QGP since $c\bar{c}$ meson states should no longer be formed due to color screening [5,6]. However, the suppression of J/Ψ and Ψ' mesons in the high density phase of nucleus-nucleus collisions at SPS energies [7–11] might also be attributed to inelastic comover scattering (cf. [12–19] and Refs. therein) provided that the corresponding J/Ψ-hadron cross sections are in the order of a few mb [20–27]. Theoretical estimates here differ by more than an order of magnitude [28] especially with respect to J/Ψ-meson scattering such that the question of charmonium suppression is not yet settled. On the other hand, at RHIC energies further absorption mechanisms – such as plasma screening and gluon scattering – might play a dominant role as suggested in Refs. [29,30] and also lead to a substantial reduction of the J/Ψ formation in central $Au + Au$ collisions.

On the other hand, it has been pointed out – within statistical models – that at RHIC energies the charmonium formation from open charm + anticharm mesons might become essential [31] and even exceed the yield from primary NN collisions [31,32]. However, a more schematic model by Ko et al. [33] – including the channels $J/\Psi + \pi \leftrightarrow D\bar{D}$ suggested that such channels should be still of minor importance at RHIC energies but become essential at LHC energies. A similar conclusion has been reached in Ref. [34]. One of the prevailing questions thus is, if open charm mesons and charmonia will achieve thermal and chemical equilibrium with the light mesons during the nucleus-nucleus reaction as suggested/anticipated in Refs. [35–38]. Such issues of equilibration phenomena are traditionally examined within nonequilibrium relativistic transport theory [13,39–42].

In this work we will calculate open charm and charmonium production at RHIC energies within the HSD transport approach [13,16,43] for the overall reaction dynamics using parametrizations for the elementary production channels including the charmed hadrons $D, \bar{D}, D^*, \bar{D}^*, D_s, \bar{D}_s, D_s^*, \bar{D}_s^*,\ J/\Psi, \Psi(2S), \chi_{2c}$ from NN and πN collisions. The latter parametrizations are fitted to PYTHIA calculations [44] above $\sqrt{s} = 10$ GeV and extrapolated to the individual thresholds, while the absolute strength of the cross sections is fixed by the experimental data as described in Ref. [43]. In the latter work we have calculated excitations functions for open charm mesons and charmonia including the J/Ψ suppression by dissociation with baryons and meson ('comovers') using the J/Ψ-meson cross sections from Haglin [20]. The centrality dependence for the J/Ψ survival probability has been presented in Ref. [16] for SPS ($\sqrt{s} = 17.3$ GeV) and RHIC energies ($\sqrt{s} = 200$ GeV), too, for $Pb + Pb$ or $Au + Au$ collisions, respectively. We here extend our previous works and include explicitly the backward channels 'charm + anticharm meson $\rightarrow$ charmonia + meson' employing detailed balance in a more schematic interaction model with a single parameter or matrix element $|M_0|^2$, that is fixed by the J/Ψ suppression data from the NA50 collaboration at SPS energies.

Our work is organized as follows: In Section 2 we will present the results of the HSD transport approach for charged hadrons, protons, antiprotons and elliptic flow in $Au + Au$ collisions at $\sqrt{s} = 200$ GeV in comparison to available data. This presentation

is necessary since the open and hidden charm formation and propagation proceeds in a dense and hot hadronic environment that should be sufficiently realistic. The elementary production cross sections for open charm and charmonia from baryon-baryon (BB) and meson-baryon (mB) collisions are presented in Section 3 as well as their interaction cross sections with hadrons. A phase-space model will be presented, furthermore, for the charmonium + meson dissociation cross sections that allows to implement 'detailed balance' for all channels of interest. Section 4 contains the actual calculations for the open and hidden charm degrees of freedom for $Pb + Pb$ collisions at $\sqrt{s} = 17.3$ GeV and $Au + Au$ collisions at $\sqrt{s} = 200$ GeV with particular emphasis on the novel aspect, i.e. the charmonium reformation by open charm mesons employing 'detailed balance'. A comparison to the preliminary data of the PHENIX Collaboration on J/Ψ suppression in $Au + Au$ collisions at $\sqrt{s} = 200$ GeV will be presented, too. Section 5 concludes this study with a summary and discussion of open problems.

II. CHARGED HADRONS, BARYONS, ANTIBARYONS AND COLLECTIVE FLOW

Before coming to the actual charmonium and open charm dynamics at RHIC energies we have to investigate, if the HSD transport approach based on string, quark, diquark ($q, \bar{q}, qq, \bar{q}\bar{q}$) as well as hadronic degrees of freedom performs reasonably well with respect to the abundancy of light hadrons composed of u, d, s quarks[1]. Such a test is essential since the dissociation of charmonia on baryon, antibaryons and mesons is directly proportional to their density in phase space. We recall that in HSD all newly produced hadrons have a formation time of $\tau_F = 0.8$ fm/c in their rest frame and do not interact during the 'partonic' propagation. Furthermore, hadronization is inhibited if the energy density

[1]For a more recent survey on hadron rapidity distributions from 2 to 160 A GeV in central nucleus-nucleus collisions within the HSD and UrQMD [45] transport approaches we refer the reader to Ref. [46].

– in the local rest frame – is above 1 GeV/fm^3, which roughly corresponds to the energy density for QGP formation in equilibrium at vanishing quark chemical potential μ_q. Thus 'hadrons' only exist as quark-antiquark or quark-diquark pairs at energy densities above 1 GeV/fm^3 and only can become ordinary hadrons if the system has expanded sufficiently. We note that this cut on the energy density is the only modification introduced as compared to the earlier studies in Refs. [16,43,47] and has also been included in the more recent systematic analysis in Ref. [46] from SIS to SPS energies.

In order to demonstrate the applicability of the HSD approach to nucleus-nucleus collisions at RHIC energies we show in Fig. 1 the calculated pseudo-rapidity distributions of charged hadrons (solid lines) for $Au + Au$ at $\sqrt{s} = 200$ GeV for different centrality classes in comparison to the experimental data of the PHOBOS Collaboration [48] (full points), where the error bars indicate the systematic experimental uncertainty. The open squares in the upper left figure correspond to the data from the BRAHMS Collaboration for the same centrality class [49]. We find that the HSD calculations show a small dip in $dN/d\eta$ at midrapidity for all centrality classes, which is not seen in the experimental distributions. Furthermore, the pseudo-rapidity distributions are slightly broader than the data which also might point towards an improper string fragmentation scheme in the LUND model [50] employed in HSD. We expect that this issue can be settled uniquely when high statistics data for pp reactions at RHIC energies become available. On the other hand, the overall description of the rapidity distributions is reasonable good for our present purposes.

A further question is related to the antibaryon and baryon abundancies at midrapidity that show the amount of baryon stopping and antibaryon production [51]. We mention that multi-meson fusion channels play a sizeable role in recreating baryon-antibaryon pairs [47,52,53] and reducing the number of light mesons accordingly. Thus detailed balance on the many-particle level – as only found more recently [47] – leads to an approximate chemical equilibrium of antibaryons with mesons whenever the meson density is sufficiently high as e.g. in nonperipheral $Au + Au$ collisions at RHIC energies. Our numerical results for the $(\bar{p} + \bar{\Lambda})/(p + \Lambda)$ ratio in 10% central $Au + Au$ collisions at $\sqrt{s} = 200$ GeV

are displayed in Fig. 2 as a function of rapidity y in comparison to the data from the BRAHMS Collaboration [54], that correspond to the measured $\bar{p}/p$ ratio, however, include some still unknown fraction from Λ and $\bar{\Lambda}$ decays. The comparison in Fig. 2 thus suffers from a 5–10% systematic uncertainty. We mention that (within statistics) practically the same rapidity distribution for antiprotons is obtained when discarding baryon-antibaryon annihilation as well as the backward channels. Thus the calculations for charmonia and open charm mesons in Section 4 will be performed in the latter limit. Nevertheless, Fig. 2 suggests that the antiproton/proton ratio is reasonably described in the HSD approach. This also holds for the net proton $(p - \bar{p})$ rapidity distribution as seen from Fig. 3 in comparison to the preliminary data of the BRAHMS Collaboration [55] for the same event class as in Fig. 2[2].

In principle, one might argue that a transport approach based on string and hadronic degrees of freedom should not be adequate in the initial stage of nucleus-nucleus collisions at RHIC energies where a new state of matter, i.e. a quark-gluon plasma (QGP), is expected/hoped to be formed. However, the global event characteristics and particle abundancies from SIS to RHIC energies are found experimentally to show a rather smooth evolution with bombarding energy [56,57] such that no obvious conclusion on the effective degrees of freedom in the initial phase can presently be drawn. Moreover, the large pressure needed to describe the elliptic flow at RHIC energies is approximately described by 'early' hadron formation – as in HSD – and the 'large' hadronic interaction cross sections. This is demonstrated in Fig. 4 where we show the calculated elliptic flow v_2 for charged hadrons (solid lines) as a function of the pseudorapidity η (upper part) and as a function of the number of 'participating nucleons' N_{part} (lower part) for $|\eta| \leq 1$ in comparison to the preliminary 'hit-based analysis' data of the PHOBOS Collaboration [58]. Note, that the experimental error bars correspond to 1σ statistical errors, only.

[2]The experimental data again include some unknown fraction of Λ and $\bar{\Lambda}$ decays such that the 'real' $(p - \bar{p})$ rapidity distribution should be slightly lower.

Our calculations underestimate the $v_2(\eta)$ distribution close to midrapidity and also are somewhat low in the centrality dependence of the elliptic flow. Whereas the elliptic flow at midrapidity is well described by hydrodynamical models, the $v_2(\eta)$ distribution comes out too flat in these calculations [59]. We note, that our HSD results are very similar to those of the hadronic rescattering model by Humanic et al. [60,61] and almost quantitatively agree with the calculations by Sahu et al. [62] performed within the hadron-string cascade model JAM [63].

On the other hand, unexpectedly high parton cross sections of $\sim$ 5–6 mb have to be assumed in parton cascades [64] in order to reproduce the elliptic flow $v_2(p_T)$ seen experimentally. These cross sections are about 1/9 of the baryon-baryon total cross section ($\sim$ 45 mb) or 1/6 of the meson-baryon cross section ($\sim$ 30 mb) such that the effective cross section for the constituent quarks and antiquarks is roughly the same in the partonic and hadronic phase. In this context it will be important to have precise data on open charm and charmonium transverse momentum (p_T) spectra since their slope might give information on the pressure generated in a possible partonic phase [65]. This argument is expected to hold especially for J/Ψ mesons since their elastic rescattering cross section with hadrons should be small in the hadronic expansion phase [66]. We note, that in central $Pb + Pb$ collisions at SPS energies the spectral slope of J/Ψ mesons is found experimentally to be substantially smaller ($\sim$ 240 MeV [67]) than that of protons ($\sim$ 300 MeV [68]). At RHIC energies the radial flow in central $Au + Au$ collisions is even larger leading to a stiffer spectrum with an inverse slope parameter $\sim$ 400 MeV for the strongly interacting protons [69].

Nevertheless, in addition to nucleus-nucleus collisions from SIS to SPS energies [46] the HSD transport approach is found to work reasonably well also at RHIC energies for the 'soft' hadron abundancies such that the 'hadronic environment' for open charm mesons and charmonia should be sufficiently realistic.

III. ELEMENTARY CROSS SECTIONS

In order to examine the dynamics of open charm and charmonium degrees of freedom during the formation and expansion phase of the highly excited system one has to know the number of initially produced particles with c or $\bar{c}$ quarks, i.e. $D, \bar{D}, D^*, \bar{D}^*, D_s, \bar{D}_s, D_s^*, \bar{D}_s^*$, $J/\Psi, \Psi(2S), \chi_{2c}$.

A. Production cross section is pp and πN collisions

In Ref. [43] we have fitted the total charmonium cross sections ($X = \chi_C, J/\Psi, \Psi'$) from NN collisions as a function of the invariant energy $\sqrt{s}$ by the function

$$\sigma_X^{NN}(s) = b_X \left(1 - \frac{m_X}{\sqrt{s}}\right)^{\alpha} \left(\frac{m_X}{\sqrt{s}}\right)^{-\beta} \Theta(\sqrt{s} - \sqrt{s_0}) \tag{1}$$

with $\alpha = 10$, $\beta = 1$, while $\sqrt{s_0}$ denotes the threshold in vacuum. The parameters were fixed in [43] to describe the J/Ψ and Ψ' data at lower energy ($\sqrt{s} \leq 30$ GeV). For our present study we use the same parametrization (1) with a slightly modified parameter $\beta = 0.775$ (instead of $\beta = 1$) in order to fit the preliminary data point from the PHENIX Collaboration [70] at $\sqrt{s} = 200$ GeV, which gives $\sigma(pp \to J/\Psi + X) = 3.8 \pm 0.6(\text{stat.}) \pm 1.3(\text{sys.})$ μb for the total J/Ψ cross section. The parameter $b_X = 240\, C_X$ nb is proportional to the fraction of charmonium states C_X. We choose $C_{\chi_C} = 0.4,\ C_{J/\Psi} = 0.46,\ C_{\Psi'} = 0.14$ in line with Ref. [71].

For the total charmonium cross sections from πN reactions we adopt the parametrization (in line with Ref. [14]):

$$\sigma_X^{\pi N}(s) = d_X \left(1 - \frac{m_X}{\sqrt{s}}\right)^{\gamma} \tag{2}$$

with $\gamma = 7.3$ and $d_x = 1360.8\ C_X$ nb, which describes the existing experimental data at low $\sqrt{s}$ reasonably well (cf. Fig. 3 from [43]).

Apart from the total cross sections, we also need the differential distribution of the produced mesons in the transverse momentum p_T and the rapidity y (or Feynman x_F) from each individual collision. We recall that $x_F = p_z/p_z^{max} \approx 2p_z/\sqrt{s}$ with p_z denoting

the longitudinal momentum. For the differential distribution in x_F from NN and πN collisions we use the ansatz from the E672/E706 Collaboration [72]:

$$\frac{dN}{dx_F dp_T} \sim (1 - |x_F|)^c \ \exp(-b_{p_T} p_T), \tag{3}$$

where $b_{p_T} = 2.08$ GeV^{-1} and $c = a/(1 + b/\sqrt{s})$. The parameters a, b are choosen as $a_{NN} = 13.5$, $b_{NN} = 24.9$ for NN collisions and $a_{\pi N} = 4.11$, $b_{\pi N} = 10.2$ for πN collisions.

In Fig. 5 (upper part) we compare the calculated J/Ψ differential cross section in rapidity y_{cm} – multiplied by the branching ratio to dileptons – with the preliminary data from the PHENIX Collaboration [70] for pp collisions at $\sqrt{s} = 200$ GeV using $\beta = 0.775$. Our elementary J/Ψ formation is seen to be in sufficient agreement with the preliminary data [70] though the rapidity distribution appears slightly broader than the data.

The number of primary J/Ψ mesons formed in central $Au + Au$ reactions at $\sqrt{s} =$ 200 GeV can be estimated – on the basis of the Glauber model – by multiplying the pp production cross section with the number of binary collisions ($N_{bin} \approx 1.2 \times 10^3$) and dividing by the inelastic pp cross section ($\sim$ 45 mb). This leads to a multiplicity of primary J/Ψ's of ~ 0.1 in very central $Au + Au$ collisions.

The total and differential cross sections for open charm mesons from pp collisions, furthermore, are taken as in Ref. [43]. They also might have to be reduced slightly as the charmonia cross sections, however, no experimental constraint is available so far. We thus refer to the results of Ref. [43] which give $\sim$16 $D\bar{D}$ pairs in central $Au + Au$ collisions at $\sqrt{s} = 200$ GeV, a factor of $\sim$160 relative to the expected primordial J/Ψ multiplicity of ~ 0.1. Note, that at $\sqrt{s} \approx 17.3$ GeV the primary $D\bar{D}$ to J/Ψ ratio is about 40 [43]; the increase of this ratio by a factor of ~ 4 from $\sqrt{s} = 17.3$ GeV to $\sqrt{s} = 200$ GeV is within the expected range. Our results for the rapidity distribution of open charm mesons from pp collisions at $\sqrt{s} = 200$ GeV (summing up all D and $\bar{D}$ mesons) is displayed in the lower part of Fig. 5 and shows a rather flat distribution at midrapidity, too. Presently, there are no data that could control this open charm rapidity spectrum.

Apart from primary hard NN collisions the open charm mesons or charmonia may also be generated by secondary 'meson'-'baryon' (mB) reactions. Here we include all

secondary collisions of mesons with 'baryons' by assuming that the open charm cross section (from Section 2 of Ref. [43]) only depends on the invariant energy $\sqrt{s}$ and not on the explicit meson or baryon state. Furthermore, we take into account all interactions of 'formed' mesons – after a formation time of $\tau_F = 0.8$ fm/c (in their rest frame) [74] – with baryons or diquarks, respectively. As pointed out in Ref. [43] the production of open charm pairs in central $Au + Au$ collisions by mB reactions is expected to be on the 10% level.

In order to study the effect of rescattering we tentatively adopt the following dissociation cross sections of charmonia with baryons independent on the energy (in line with Refs. [16,43]):

$$\sigma_{c\bar{c}B} = 6 \text{ mb}; \ \sigma_{J/\Psi B} = 4 \text{ mb}; \ \sigma_{\chi_c B} = 5 \text{ mb}; \ \sigma_{\Psi' B} = 10 \text{ mb}. \tag{4}$$

In (4) the cross section $\sigma_{c\bar{c}B}$ stands for a (color dipole) pre-resonance ($c\bar{c}$) - baryon cross section, since the $c\bar{c}$ pair produced initially cannot be identified with a particular hadron due to the uncertainty relation in energy and time. For the lifetime of the pre-resonance $c\bar{c}$ pair (in it's rest frame) a value of $\tau_{c\bar{c}} = 0.3$ fm/c is assumed following Ref. [75]. This value corresponds to the mass difference of the Ψ' and J/Ψ.

For $D, D^*, \bar{D}, \bar{D}^*$ - meson $(\pi, \eta, \rho, \omega)$ scattering we address to the calculations from Ref. [22,23] which predict elastic cross sections in the range of 10–20 mb depending on the size of the formfactor employed. As a guideline we use a constant cross section of 10 mb for elastic scattering with mesons and also baryons, although the latter might be even higher for very low relative momenta.

B. Comover dissociation channels

As already pointed out in the introduction the J/Ψ formation cross sections by open charm mesons or the inverse comover dissociation cross sections are not well known and the significance of these channels is discussed controversely in the present literature [28,31,32,34,76,77]. Whereas in Refs. [16,43] the energy-dependent J/Ψ-meson cross

sections for dissociation to $D\bar{D}$ have been taken from the calculations of Haglin [20], we here introduce a simple 2-body transition model with a single free parameter M_0^2, that allows to implement the backward reactions uniquely by employing detailed balance for each individual channel. Since the meson-meson dissociation and backward reactions typically occur with low relative momenta ('comovers') it is legitimate to write the cross section for the process $m_1 + m_2 \to m_3 + m_4$ as

$$\sigma_{1+2\to 3+4}(\sqrt{s}) = 2^4 \ \frac{E_1 E_2 E_3 E_4}{s} \ |M_f|^2 \ \left(\frac{M_3 + M_4}{\sqrt{s}}\right)^6 \ \frac{P_f}{P_i}, \tag{5}$$

where E_i and S_i denote the energy and spin of hadron i, respectively. The initial and final momenta for fixed invariant energy $\sqrt{s}$ are given by

$$P_i^2 = \frac{(s-(M_1+M_2)^2)(s-(M_1-M_2)^2)}{4s}, \ P_f^2 = \frac{(s-(M_3+M_4)^2)(s-(M_3-M_4)^2)}{4s}, \tag{6}$$

where M_i denotes the mass of hadron i. In (5) $|M_f|^2$ stands for the effective matrix element squared which for the different 2-body channels is taken of the form

$$\begin{aligned}
|M_f|^2 &= M_0^2 \qquad && \text{for } (\pi,\rho) + J/\Psi \to D + \bar{D} \\
|M_f|^2 &= 3M_0^2 \qquad && \text{for } (\pi,\rho) + J/\Psi \to D^* + \bar{D}, D + \bar{D}^*, D^* + \bar{D}^* \\
|M_f|^2 &= \tfrac{1}{3}M_0^2 \qquad && \text{for } (K,K^*) + J/\Psi \to D_s + \bar{D}, \bar{D}_s D \\
|M_f|^2 &= M_0^2 \qquad && \text{for } (K,K^*) + J/\Psi \to D_s + \bar{D}^*, \bar{D}_s D^*, D_s^* + \bar{D}, \bar{D}_s^* D, \bar{D}_s^* D^*
\end{aligned} \tag{7}$$

involving a single parameter M_0^2 to be fixed at SPS energies in comparison to the data of the NA50 Collaboration [9,10]. The relative factors of 3 in (7) are guided by the sum rule studies in [78] which suggest that the cross section is increased whenever a vector meson D^* or $\bar{D}^*$ appears in the final channel while another factor of 1/3 is introduced for each s or $\bar{s}$ quark involved. The factor $((M_3+M_4)/\sqrt{s})^6$ in (5) accounts for the suppression of binary channels with increasing $\sqrt{s}$ and has been fitted to the experimental data for the reactions $\pi + N \to \rho + N, \omega + N, \Phi + N, K^+ + \Lambda$ in Ref. [79]. For simplicity we use the same matrix elements for the dissociation of χ_c and Ψ' with mesons though there is no fundamental reason why these matrix elements should be the same. However, since we

here concentrate only on the net J/Ψ absorption and production and not on the explicit charmonium 'chemistry', this approximation should work out reasonably well within the range of systematic uncertainties.

The advantage of the model introduced in (5) is that detailed balance for the binary reactions can be employed strictly for each individual channel, i.e.

$$\sigma_{3+4\rightarrow 1+2}(\sqrt{s}) = \sigma_{1+2\rightarrow 3+4}(\sqrt{s}) \; \frac{(2S_1+1)(2S_2+1)}{(2S_3+1)(2S_4+1)} \; \frac{P_i^2}{P_f^2}, \tag{8}$$

and the role of the backward reactions (J/Ψ+meson formation by $D+\bar{D}$ flavor exchange) can be explored without introducing any additional parameter once M_0^2 is fixed. The uncertainty in the cross sections (5) is of the same order of magnitude as that in Lagrangian approaches using e.g. $SU(4)_{flavor}$ symmetry [22,23] since the formfactors at the vertices are essentially unknown [78].

As mentioned before, we fit the parameter M_0^2 to the J/Ψ suppression data from the NA50 Collaboration for $Pb+Pb$ collisions at 160 A GeV (cf. Section 4.1). For the value $M_0^2 = 0.13$ fm/GeV^2 used below we end up with the J/Ψ dissociation cross sections

$$\sigma_{J/\Psi+m\rightarrow X}(\sqrt{s}) = \sum_c \sigma_{J/\Psi+m\rightarrow c}(\sqrt{s}) \tag{9}$$

displayed in Fig. 6 with π, ρ, K and K^* mesons. The summation over the final channel c in (9) includes all binary channels compatible with charm quark and charge conservation. Note, that for the comover absorption scenario essentially the regime 3.8 GeV $\leq \sqrt{s} \leq$ 4.8 GeV is of relevance (cf. Fig. 7.13 in [13]) where the dissociation cross sections are on the level of a few mb. We note, that the explicit channel $J/\Psi + \pi \rightarrow D + \bar{D}$, which has often been calculated in the literature [22,23,76,77] is below 0.7 mb in our model. A somewhat more essential result is that the J/Ψ dissociation cross section with ρ-mesons is in the order of 5-7 mb as in the calculations of Haglin [20] used before in Ref. [43], since this channel was found to dominate the J/Ψ dissociation at SPS energies [13]. The explicit shape of the cross sections is characterized by a rapid rise in $\sqrt{s}$ whenever a new channel opens up. On the other hand, the channels with vector mesons (ρ, K^*) are 'exothermal' and thus divergent at threshold.

The cross sections for the backward channels $D+\bar{D}, D+\bar{D}^*, D^*+\bar{D}, D^*+\bar{D}^* \to J/\Psi$ + meson as well as the channels involving s or $\bar{s}$ quarks, i.e. $D_s+\bar{D}, D_s+\bar{D}^*, D_s^*+\bar{D}, D_s^*+\bar{D}^+ \to J/\Psi+(K,K^*)$, then are fixed by detailed balance via (8). The actual results for these channels – summed up again over all possible binary final states – are displayed in Fig. 7 separately for the 'non-strangeness' (upper part) and 'strangeness' channels (lower part) showing again divergent cross sections for 'exothermal' channels like $D+\bar{D} \to J/\Psi+\pi$. Such divergent cross sections arise in all 'exothermal' S-wave channels implying that $D+\bar{D}$ or $D^*+\bar{D}$ mesons with low relative momentum have a large cross section for c and $\bar{c}$ quark exchange. In actual transport calculations such divergent cross sections impose no problems since the transition rates $\sim P_f \sigma_{3+4\to 1+2}$ remain finite, as it is easily seen when inserting (5) into (8), since the divergent factor P_f^2 cancels out. Furthermore, in the transport calculations an explicit cut in the total cross sections of 120 mb is employed, which simulates the screening of large cross sections at finite hadron density.

C. Numerical implementation

We recall that (as in Refs. [43,73,80,81]) the charm degrees of freedom are treated perturbatively and that initial hard processes (such as $c\bar{c}$ or Drell-Yan production from NN collisions) are 'precalculated' to achieve a scaling of the inclusive cross section with the number of projectile and target nucleons as $A_P \times A_T$ when integrating over impact parameter. To implement this scaling we separate the production of the hard and soft processes: The space-time production vertices of the $c\bar{c}$ pairs are 'precalculated' in each transport run by neglecting the soft processes, i.e. the production of light quarks and assosiated mesons, and then reinserted in the dynamical calculation at the proper space-time point during the actual calculation that includes all soft processes. As shown in Ref. [43] this prescription is very well in line with Glauber calculations for the production of hard probes at fixed impact parameter, too. We mention that this 'precalculation' of $c\bar{c}$ production might be modified at RHIC energies due to changes of the gluon structure

functions during the heavy-ion reaction or related shadowing phenomena [82]. Such effects, however, are expected to be of minor importance at RHIC energies (and below) and will be discarded for our present study, that concentrates on the balance between comover absorption and J/Ψ reproduction channels.

Each open charm meson and charm vector meson is produced in the transport calculation with a weight W_i given by the ratio of the actual production cross section divided by the inelastic nucleon-nucleon cross section, e.g.

$$W_i = \frac{\sigma_{NN\to J/\Psi+x}(\sqrt{s})}{\sigma_{NN}^{inelas.}(\sqrt{s})}. \tag{10}$$

In the transport simulation we follow the motion of the charmonium pairs or produced $D, \bar{D}, D^*, \bar{D}^*$-mesons within the full background of strings/hadrons by propagating them as free particles, i.e. neglecting in-medium potentials, but compute their collisional history with baryons and mesons or quarks and diquarks. For reactions with diquarks we use the corresponding reaction cross section with baryons multiplied by a factor of 2/3. For collisions with quarks (antiquarks) we adopt half of the cross section for collisions with mesons.

Furthermore, in addition to our previous studies [16,43,81] the recreation of charmonia by channels such as $D^* + \bar{D} \to J/\Psi + \pi$ etc. is taken into account in each individual run according to the cross sections (8) with the weight of the produced charmonium states k given by

$$W_k = W_i W_j, \tag{11}$$

where W_i, W_j are the individual weights of the open charm mesons. The open charm mesons are not allowed to rescatter within a formation time of 0.3 fm/c (in their rest frame) since a finite time is needed to form their wave functions. This formation time is not well known and presently can only be estimated. Thus we checked – by performing calculations with formation times from 0.3 to 0.6 fm/c – that the physical statements (see below) remain robust. As commonly employed in transport simulations, the open charm meson pairs, that stem from the same interaction vertex, are not allowed to rescatter with each other again unless an intermediate scattering has occurred.

IV. NUCLEUS-NUCLEUS COLLISIONS

A. SPS energies

We directly step on with the results for the charmonium suppression and start with the system $Pb + Pb$ at 160 A GeV to demonstrate that the 'late' comover dissociation model (5) is approximately in line with the data of the NA50 Collaboration. The corresponding J/Ψ suppression (in terms of the $\mu^+\mu^-$ decay branch relative to the Drell-Yan background from 2.9 – 4.5 GeV invariant mass) as a function of the transverse energy E_T in $Pb + Pb$ collisions at 160 A GeV is shown in Fig. 8. The solid line (HSD'03) stands for the HSD result within the comover absorption scenario for the cross sections defined by (5) while the various data points reflect the different data releases from the NA50 Collaboration [7–10]. Note, that the 2002 data [11] (lower part) no longer indicate the drop at the highest E_T (for analysis B) in line with the HSD calculations from 1997 [81] and the UrQMD results from 1999 [18] (dashed histogram). We mention that the present calculation (solid line, HSD'03) agrees with the earlier calculations from Ref. [81] (dotted line, HSD'97) very well except for the first E_T-bin. Thus the cross sections presented in Fig. 6 do not lead to an overestimation of J/Ψ suppression at SPS energies. There might be alternative explanations for J/Ψ suppression as discussed in Refs. [14,29,30,73,83] and/or further dissociation mechanism not considered here. However, for the purposes of the present study it is sufficient to point out that the cross sections displayed in Fig. 6 most likely are upper limits.

In order to provide some information on the relative production and absorption channels for charmonia in these reactions we show the calculated J/Ψ rapidity distributions for 10% central $Pb + Pb$ collisions at $\sqrt{s} = 17.3$ GeV in Fig. 9. The ordering of the different lines is as follows: the upper dot-dot-dashed line stands for the rapidity distribution of J/Ψ mesons produced by initial BB collisions while the lowest dot-dashed line reflects the rapidity distribution of J/Ψ mesons from secondary mB collisions that are of minor importance at SPS energies. The dashed line corresponds to the J/Ψ's dissociated by

baryons (B); this absorption mechanism is denoted as 'conventional J/Ψ attenuation' by the NA50 Collaboration and also present in $p + A$ reactions. The dotted line ('m abs.') gives the rapidity distribution for J/Ψ's dissociated with mesons ('comover absorption') while the full solid line stands for the final J/Ψ rapidity distribution.

As mentioned in Section 3, the model (5) allows to calculate the backward channels – leading to J/Ψ reformation by open charm + anticharm mesons – without introducing any new parameter or assumption. The result for the total J/Ψ comover absorption rate (solid histogram) in central $Pb + Pb$ collisions at 160 A GeV is shown in Fig. 10 in comparison to the J/Ψ reformation rate (dashed histogram) that includes all backward channels. Since the rates differ by about 2 orders of magnitude, the backward rate for J/Ψ formation can clearly be neglected at SPS energies even for central $Pb+Pb$ reactions. This result is essentially due to the fact that the expected multiplicity of open charm pairs is ~ 0.12 in central $Pb + Pb$ collisions at $\sqrt{s} = 17.3$ GeV (according to the calculations in Ref. [43]). Even in case of 'open charm enhancement' (as suggested in Ref. [84]) by a factor ~ 3, where the J/Ψ reformation rate would increase by a factor ~ 9, the backward channels still could be neglected.

Since the 'comover' dissociation cross sections employed should be regarded as upper limits, we conclude that no chemical equilibration between mesons, open charm mesons and charmonia is achieved dynamically at SPS energies. Note, however, that the transverse mass M_T spectra for all mesons including open charm and charmonia from central $Pb + Pb$ collisions scale according to the HSD calculations (cf. Fig. 18 of Ref. [43]), if final state elastic scatterings are omitted. Thus statistical model fits still should work for the different hadron abundancies.

B. RHIC energies

For central $Au + Au$ collisions at $\sqrt{s} = 200$ GeV, however, the multiplicity of open charm pairs should be ~ 16, i.e. by about 2 orders of magnitude larger, such that a much higher J/Ψ reformation rate ($\sim N^2_{c\bar{c}}$) is expected at RHIC energies (cf. Ref. [30]). In Fig.

11 we display the total J/Ψ comover absorption rate (solid histogram) in comparison to the J/Ψ reformation rate (dashed histogram) as a function of time in the center-of-mass frame. Contrary to Fig. 10 now the two rates become comparable for $t \geq$ 4-5 fm/c and suggest that at the full RHIC energy of $\sqrt{s} = 200$ GeV the J/Ψ comover dissociation is no longer important since the charmonia dissociated in this channel are approximately recreated in the backward channels. Accordingly, the J/Ψ dissociation at RHIC should be less pronounced than at SPS energies. Moreover, there is even a small excess of J/Ψ formation by $D + \bar{D}$ reactions in the first 2 fm/c qualitatively in line with AMPT calculations by Zhang et al. [85].

In order to provide some information on the relative production and absorption channels for charmonia in these reactions we show – in analogy to Fig. 9 – the calculated J/Ψ rapidity distributions for 12% central $Au + Au$ collisions at $\sqrt{s} = 200$ GeV in the upper part of Fig. 12. The ordering of the different lines is as follows: the upper dot-dot-dashed line stands for the rapidity distribution of J/Ψ mesons produced by initial BB collisions while the lowest dot-dashed line reflects the rapidity distribution of J/Ψ mesons from secondary mB collisions that are of minor importance also at RHIC energies. The dashed line corresponds to the J/Ψ's dissociated by baryons (B) and corresponds to the 'conventional J/Ψ attenuation'. This distribution is approximately the same as the recreation of J/Ψ's from $D + \bar{D}$ annihilation (thin solid line with open circles). The dotted line ('m abs.') gives the rapidity distribution for J/Ψ's dissociated with mesons ('comover absorption'); it is slightly lower than the $D + \bar{D}$ recreation channel. The full solid line stands for the final J/Ψ rapidity distribution which is about a factor of ~ 3 lower than the primary production from BB collisions. Since all distributions (within statistics) are practically flat for $|y_{cm}| \leq 2$ no strong sensitivity of the J/Ψ survival probability is expected for different rapidity cuts in this interval around midrapidity.

We additionally comment on results of HSD calculations that have been performed under the assumption of initial J/Ψ 'melting' by color screening in a QGP phase as advocated in Refs. [5,6]. To this aim we have 'deleted' all charmonia created initially from primary BB collisions in the calculation, but evolved the system in time with the

same production and absorption cross sections as before. The resulting final J/Ψ rapidity distribution for central $Au + Au$ collisions at $\sqrt{s} = 200$ GeV is shown in the lower part of Fig. 12 by the dashed line in comparison to the final J/Ψ rapidity distribution from the upper part of the figure (solid line). The comparison demonstrates that even in case of complete initial charmonium dissociation a finite amount of J/Ψ's should be seen experimentally, which is roughly half of the yield expected from the full calculations and essentially due to the $D+\bar{D}$ production channels. Since the latter cross sections are upper estimates, the J/Ψ yield (dashed line in Fig. 12) also has to be considered as an upper limit in this case.

A note of caution should be added in context with Fig. 12 since the actual rapidity distributions might change quantitatively when including a more refined model for the matrix elements in (7) especially for the χ_c and Ψ' states. Furthermore, in-medium modifications (or self-energy corrections) of the open charm mesons (and charmonia) should change the final rapidity distributions to some extent since a lowering of $D, \bar{D}$ masses leads to an increase of J/Ψ + meson absorption rates and a decrease of the backward channel rates [85]. For constant matrix elements as in (7) these modifications directly result from an enhanced phase space for absorption and a reduced invariant energy for the backward channels. On the other hand, for enhanced $D, \bar{D}$ masses in the medium the J/Ψ + meson absorption rates will be lowered and the backward channels be enhanced accordingly. As argued in Ref. [86] charmonium spectroscopy in $\bar{p}$ induced reactions on nuclei might shed some further light on this presently open issue. Nevertheless, our actual results for the J/Ψ reformation by open charm + anticharm mesons are in qualitative and even quantitative agreement with the independent transport studies in Ref. [85] that also demonstrate a net reduction of J/Ψ mesons relative to the extrapolations from pp collisions with the number of binary collisions.

We now turn back again to the HSD results for the full calculations. To quantify the final J/Ψ suppression in $Au + Au$ collisions at RHIC we show in Fig. 13 the calculated J/Ψ survival probability $S_{J/\Psi}$ defined as

$$S_{J/\Psi} = \frac{N_{fin}^{J/\Psi}}{N_{BB}^{J/\Psi}}, \tag{12}$$

where $N_{fin}^{J/\Psi}$ and $N_{BB}^{J/\Psi}$ denote the final number of J/Ψ mesons and the number of J/Ψ's produced initially by BB reactions, respectively. In Fig. 13 the quantity (12) is displayed as a function of the transverse energy E_T – in units of the transverse energy at impact parameter $b = 1$ fm – for $Au + Au$ collisions with (solid line) and without inclusion of the backward channels (dash-dotted line). In fact, the dash-dotted line is (within statistics) identical to the previous calculation in Ref. [16] demonstrating a considerable J/Ψ 'comover' suppression for central collisions. When including the reformation channels this suppression is substantially reduced and leads to a less effective dissociation of charmonia than at SPS energies (middle dashed line). Furthermore, we observe that $S_{J/\Psi} \leq 1$ for all centralities and thus no J/Ψ enhancement relative to the primary BB production is found from our calculations as claimed in the statistical models of Refs. [31,38,87]. We also like to recall that the charmonium 'melting scenario' advocated in Ref. [83] should lead to a step-like E_T dependence of $S_{J/\Psi}$ due to a successive melting of the χ_c and J/Ψ and an almost complete disappearance of J/Ψ's for central collisions. Moreover, as shown in Refs. [88,89], statistical models on the partonic or even hadronic level lead to very different predictions for the J/Ψ multiplicity as a function of centrality in $Au + Au$ collisions at $\sqrt{s} = 200$ GeV. Since at RHIC energies the predictions of the 'comover' approach, the statistical models and the 'melting scenario' are substantially different, experiment should clearly decide about the adequacy of the concepts involved.

The preliminary data of the PHENIX Collaboration [70] allow for a first glance at the situation encountered in $Au + Au$ collisions at $\sqrt{s} = 200$ GeV. In order to compare with the preliminary data we have performed a rapidity cut $|y_{cm}| \leq 2$ in the calculations. In Fig. 14 the J/Ψ multiplicity per binary collision (times the branching ratio B) is shown as a function of the number of participating nucleons A_{part} in comparison to the data at midrapidity. Whereas our transport results give a monotonous decrease of the J/Ψ yield (per binary collision) with centrality, the statistical charm coalescence model of Gorenstein et al. [89] predicts an increase by about 20% from $A_{part} = 100$ to 380. Since

the statistics (and binning in A_{part}) is quite limited so far on the experimental side, no final conclusion can presently be drawn, however, the data neither suggest a dramatic enhancement of J/Ψ production nor a complete 'melting' of the charmonia in the QGP phase.

V. SUMMARY

In this work we have performed a first comparison of results from HSD transport calculations on meson, baryon, antibaryon production and elliptic flow with the (preliminary) data for $Au + Au$ collisions at $\sqrt{s} = 200$ GeV from the PHOBOS, BRAHMS and PHENIX Collaborations. The HSD transport approach, which is based on quark, diquark, string and hadronic degrees of freedom, is found to give a quite reasonable description of the different observables studied in this work. Only the elliptic flow v_2 is underestimated closer to midrapidity – quantitatively in line with the hadron-string cascade calculations in Ref. [62] – indicating that there might be 'extra pressure' being generated in the 'prehadronic phase'.

On the other hand, hard probes such as charmonia and open D-meson pairs are expected to be sensitive to the initial phase of high energy density where charmonia might be 'melting' according to the scenario advocated in Ref. [83], their formation be suppressed due to plasma screening [33] or absorbed early by neighboring strings [73]. However, charmonia might also be generated in a statistical fashion at the phase boundary between the QGP and an interacting hadron gas such that their abundance could be in statistical (chemical) equilibrium with the light and strange hadrons [35,87]. The latter picture is expected to lead not to a suppression but to an enhancement of J/Ψ mesons at the full RHIC energy if compared to the scaled J/Ψ multiplicity from pp collisions [31]. We recall that the 'hadronic comover' dissociation concept has lead to a ~ 90 % J/Ψ suppression in central $Au + Au$ collisions at $\sqrt{s}$ [16] due to the high meson densities encountered, however, as pointed out in [16], the latter calculations had been performed without including the backward $D + \bar{D} \rightarrow J/\Psi +$ meson channels thus violating 'detailed

balance'.

The focus of this work has been to show the dynamical effects from the backward channels for charmonium reproduction by $D + \bar{D}$ channels employing detailed balance on a microscopic level. To this aim we have formulated a simple phase-space model for the individual charmonium dissociation channels with a single free parameter M_0^2 (cf. Section 3), which we have fixed at SPS energies in comparison to the J/Ψ suppression data of the NA50 Collaboration. In fact, the results for the charmonium suppression are practically the same as in the previous HSD transport calculations [16,43,81]. From our dynamical calculations we find that the charmonium recreation by the backward channels plays no role at SPS energies (cf. Fig. 10), however, becomes substantial in $Au + Au$ collisions at $\sqrt{s} = 200$ GeV and even is slightly larger than the 'comover' absorption channel. This leads to the final result that the total J/Ψ suppression as a function of centrality is less pronounced than at SPS energies, where the backward channels play no role. Furthermore, even in case that all directly produced J/Ψ mesons are not formed as a mesonic state (e.g. due to color screening), a sizeable amount of charmonia is found asymptotically due to the $D+\bar{D} \rightarrow J/\Psi$ + meson channels which is almost quantitatively in line with the AMPT calculations in Ref. [85] for central $Au+Au$ collisions at $\sqrt{s} = 200$ GeV. Since the cross sections for J/Ψ + meson absorption employed in this work have to be considered as upper limits, the charmonium reformation by $D + \bar{D} \rightarrow J/\Psi$ + meson channels should be lower than the J/Ψ cross section expected from binary scaling of pp reactions. The preliminary data of the PHENIX Collaboration [70] are compatible with our full transport calculations (cf. Fig. 14), however, improved statistics and also data for light systems such as $Ne + Ne$ and $Ag + Ag$ will be necessary to clarify the issue of charmonium suppression experimentally.

ACKNOWLEDGEMENTS

The authors acknowledge inspiring discussions with M. Bleicher, C. Greiner and A. P. Kostyuk. Furthermore, they like to thank J. J. Gaardhoje for providing the experimental data of the BRAHMS Collaboration in Fig. 2.

REFERENCES

[1] Quark Matter '01, Nucl. Phys. **A698**, 1 (2001).

[2] S. A. Bass, M. Gyulassy, H. Stöcker, and W. Greiner, J. Phys. **G 25**, R1 (1999).

[3] M. Reiter, E. L. Bratkovskaya, M. Bleicher, W. Bauer, W. Cassing, H. Weber, and H. Stöcker, nucl-th/0301067, to appear in Nucl. Phys. **A**.

[4] U. Heinz, Nucl. Phys. **A 661**, 140c (1999).

[5] T. Matsui and H. Satz, Phys. Lett. **B178**, 416 (1986).

[6] H. Satz, Rep. Progr. Phys. **63**, 1511 (2000).

[7] M. C. Abreu et al., NA50 collaboration, Phys. Lett. **B410**, 337 (1997).

[8] M. C. Abreu et al., NA50 collaboration, Phys. Lett. **B444**, 516 (1998).

[9] M. C. Abreu et al., NA50 collaboration, Phys. Lett. **B477**, 28 (2000).

[10] M. C. Abreu et al., NA50 collaboration, Phys. Lett. **B450**, 456 (1999).

[11] L. Ramello et al., NA50 collaboration, Quark Matter 2002, Nantes, France (unpublished).

[12] A. Capella, E. G. Ferreiro, and A. B. Kaidalov, Phys. Rev. Lett. **85**, 2080 (2000).

[13] W. Cassing, E. L. Bratkovskaya, Phys. Rep. **308**, 65 (1999).

[14] R. Vogt, Phys. Rep. **310**, 197 (1999).

[15] C. Gerschel and J. Hüfner, Ann. Rev. Nucl. Part. Sci. **49**, 255 (1999).

[16] W. Cassing, E. L. Bratkovskaya, and S. Juchem, Nucl. Phys. **A674**, 249 (2000).

[17] C. Spieles, R. Vogt, L. Gerland, S. A. Bass, M. Bleicher, H. Stöcker, and W. Greiner, J. Phys. G **25**, 2351 (1999).

[18] C. Spieles, R. Vogt, L. Gerland, S. A. Bass, M. Bleicher, H. Stöcker, and W. Greiner, Phys. Rev. C **60**, 054901 (1999).

[19] L. Gerland, L. Frankfurt, M. Strikman, H. Stöcker, and W. Greiner, Nucl. Phys. **A663**, 1019 (2000).

[20] K. L. Haglin, Phys. Rev. C **61**, 031903 (2000).

[21] K. L. Haglin and C. Gale, Phys. Rev. C **63**, 065201 (2001).

[22] Z. Lin and C. M. Ko, Phys. Rev. C **62**, 034903 (2000).

[23] Z. Lin and C. M. Ko, J. Phys. G **27**, 617 (2001).

[24] A. Sibirtsev, K. Tsushima, and A. W. Thomas, Phys. Rev. C **63**, 044906 (2001).

[25] A. Sibirtsev, K. Tsushima, K. Saito, and A. W. Thomas, Phys. Lett. **B484**, 23 (2000).

[26] C. Y. Wong, Phys. Rev. C **65**, 034902 (2002).

[27] C. R. G. Burau, D. B. Blaschke, and Y. L. Kalinovsky, Phys. Lett. B **506**, 297 (2001).

[28] B. Müller, Nucl. Phys. **A661**, 272c (1999).

[29] B. Zhang, C. M. Ko, B.-A. Li, Z. Lin, B.-H. Sa, Phys. Rev. C **62**, 054905 (2000).

[30] L. Grandchamp and R. Rapp, Phys. Lett. **B523**, 60 (2001); Nucl. Phys. **A709**, 415 (2002).

[31] R. L. Thews, M. Schroedter, and J. Rafelski, Phys. Rev. C **63**, 054905 (2001).

[32] P. Braun-Munzinger and J. Stachel, Phys. Lett. **B490**, 196 (2000).

[33] C. M. Ko, X. N. Wang, B. Zhang, and X. F. Zhang, Phys. Lett. **B444**, 237 (1998).

[34] P. Braun-Munzinger and K. Redlich, Eur. Phys. J. C **16**, 519 (2000); Nucl. Phys. **A661**, 546 (1999).

[35] M. Gazdzicki and M. Gorenstein, Phys. Rev. Lett. **83**, 4009 (1999).

[36] M. Gazdzicki, Phys. Rev. C **60**, 054903 (1999).

[37] K. Gallmeister, B. Kämpfer, and O. P. Pavlenko, Phys. Lett. **B473**, 20 (2000).

[38] M. I. Gorenstein, A. P. Kostyuk, H. Stöcker, and W. Greiner, Phys. Lett. **B509**, 277 (2001); J. Phys. G **27**, L47 (2001); A. P. Kostyuk, M. I. Gorenstein, H. Stöcker, and W. Greiner, Phys. Lett. **B531**, 195 (2002).

[39] H. Stöcker and W. Greiner, Phys. Rep. **137**, 277 (1986).

[40] W. Cassing, V. Metag, U. Mosel, and K. Niita, Phys. Rep. **188**, 363 (1990); W. Cassing and U. Mosel, Prog. Part. Nucl. Phys. **25**, 235 (1990).

[41] C. M. Ko and G. Q. Li, J. Phys. G **22**, 1673 (1996).

[42] S.A. Bass, M. Belkacem, M. Bleicher, M. Brandstetter, L. Bravina, C. Ernst, L. Gerland, M. Hofmann, S. Hofmann, J. Konopka, G. Mao, L. Neise, S. Soff, C. Spieles, H. Weber, L.A. Winckelmann, H. Stöcker, W. Greiner, Ch. Hartnack, J. Aichelin, and N. Amelin, Prog. Part. Nucl. Phys. **42**, 279 (1998).

[43] W. Cassing, E. L. Bratkovskaya, and A. Sibirtsev, Nucl. Phys. **A691**, 753 (2001).

[44] H.-U. Bengtsson and T. Sjöstrand, Comp. Phys. Commun. **46**, 43 (1987).

[45] H. Weber, M. Bleicher, L. Bravina, H. Stöcker, and W. Greiner, Phys. Lett. **B442**, 443 (1998).

[46] H. Weber, E. L. Bratkovskaya, W. Cassing, and H. Stöcker, Phys. Rev. C **67**, 014904 (2003).

[47] W. Cassing, Nucl. Phys. **A700**, 618 (2002).

[48] R. Nouicer et al., PHOBOS Collab., nucl-ex/0208003, to be published in the Proceedings of XXXVIIth Rencontres de Moriond, QCD and High Energy Hadronic Interactions, March 23rd, 2002.

[49] I. G. Bearden et al., BRAMS Collab., Phys. Rev. Lett. **88**, 202301 (2002).

[50] B. Anderson, G. Gustafson, and Hong Pi, Z. Phys. C **57**, 485 (1993).

[51] H. Weber, E. L. Bratkovskaya, and H. Stöcker, Phys. Rev. C **66**, 054903 (2002).

[52] R. Rapp and E. Shuryak, Phys. Rev. Lett. **86**, 2980 (2001) 2980; Nucl. Phys. **A698**, 587 (2002).

[53] C. Greiner and S. Leupold, J. Phys. G **27**, L95 (2001).

[54] I. G. Bearden et al., BRAHMS Collab., nucl-ex/0207006, Phys. Rev. Lett., in print.

[55] P. Christiansen et al., BRAHMS Collab., nucl-ex/0212002, to be published in the Proceeding of the XVI International Conference on Particle and Nuclei (PANIC02), Osaka, Japan, Sep. 30 - Oct. 4, 2002.

[56] J. L. Nagle and T. S. Ullrich, nucl-ex/0203007.

[57] M. D. Baker et al., PHOBOS Collaboration, nucl-ex/0212009.

[58] S. Manly et al., PHOBOS Collaboration, nucl-ex/0210036, to be published in the Proceedings of the 16th International Conference on Ultrarelativistic Nucleus-Nucleus Collisions, Nantes, France, July 18-24, 2002.

[59] T. Hirano, Phys. Rev. C **65**, 011901 (2001).

[60] T. J. Humanic, nucl-th/0203004; nucl-th/0205053.

[61] R. Bellwied, H. Caines, and T. J. Humanic, Phys. Rev. C **62**, 054906 (2000).

[62] P. K. Sahu, N. Otuka, and A. Ohnishi, nucl-th/0206010.

[63] Y. Nara, N. Otuka, A. Ohnishi, K. Niita, and S. Chiba, Phys. Rev. C **61**, 024901 (2000).

[64] Zi-wei Lin and C. M. Ko, Phys. Rev. C **65**, 034904 (2002).

[65] Nu Xu and Zhangbu Xu, nucl-ex/0211012.

[66] H. van Hecke, H. Sorge, and N. Xu, Nucl. Phys. **A661**, 493c (1999); H. Sorge, Phys. Lett. **B373**, 16 (1996).

[67] M. C. Abreu et al., NA50 Collab., Phys. Lett. **B499**, 85 (2001).

[68] I. G. Bearden et al., Phys. Rev. Lett. **78**, 2080 (1997).

[69] C. Adler et al., STAR Collab., Phys. Rev. Lett. **87**, 262302 (2001); *ibid* **89**, 092301 (2002).

[70] J. L. Nagle et al., PHENIX Collab., nucl-ex/0209015, to be published in the Proceedings of the Quark Matter 2002, Nantes, France, July 18-24, 2002 (Nucl. Phys. A).

[71] R. Gavai et al., Int. J. Mod. Phys. **A10**, 3043 (1995).

[72] V. Abramov et al., E672/E706 Collab., FERMILAB-Pub-91/62-E, IFVE-91-9, Mar. 1991.

[73] J. Geiss, C. Greiner, E. L. Bratkovskaya, W. Cassing, and U. Mosel, Phys. Lett. **B447**, 31 (1999).

[74] J. Geiss, W. Cassing, and C. Greiner, Nucl. Phys. **A644**, 107 (1998).

[75] D. Kharzeev and R. L. Thews, Phys. Rev. C **60**, 041901 (1999).

[76] K. Martins, D. Blaschke, and E. Quack, Phys. Rev. C **51**, 2723 (1995).

[77] C. Y. Wong, E. S. Swanson, and T. Barnes, Phys. Rev. C **62**, 045201 (2000); Phys. Rev. C **65**, 014903 (2002).

[78] F. O. Duraes, H. Kim, S. H. Lee, F. S. Navarra and M. Nielsen, nucl-th/0211092.

[79] W. Cassing, L. A Kondratyuk, G. I. Lykasov, and M. V. Rzjanin, Phys. Lett. **B540**, 1 (2001).

[80] W. Cassing and C. M. Ko, Phys. Lett. **B396**, 39 (1997).

[81] W. Cassing and E. L. Bratkovskaya, Nucl. Phys. **A623**, 570 (1997).

[82] J. O. Schmitt, G. C. Nayak, H. Stöcker, and W. Greiner, Phys. Lett. **B498**, 163 (2001).

[83] H. Satz, Nucl. Phys. **A661**, 104c (1999).

[84] M. C. Abreu et al., NA50 collaboration, Eur. Phys. J. C **14**, 443 (2000).

[85] B. Zhang, C. M. Ko, B.-A. Li, Z.-W. Lin, and S. Pal, Phys. Rev. C **65**, 054909 (2002).

[86] Ye. S. Golubeva, E. L. Bratkovslaya, W. Cassing, and L. A. Kondratyuk, nucl-th/0212074, Eur. Phys. J **A**, in press.

[87] P. Braun-Munzinger, D. Miskowiec, A. Dress, and C. Lourenco, Eur. Phys. J. C **1**, 123 (1998).

[88] M. I. Gorenstein, A. P. Kostyuk, H. Stöcker, and W. Greiner, Phys. Lett. **B 524**, 265 (2002).

[89] M. I. Gorenstein, A. P. Kostyuk, L. McLerran, H. Stöcker, and W. Greiner, J. Phys. **G 28**, 2151 (2002).

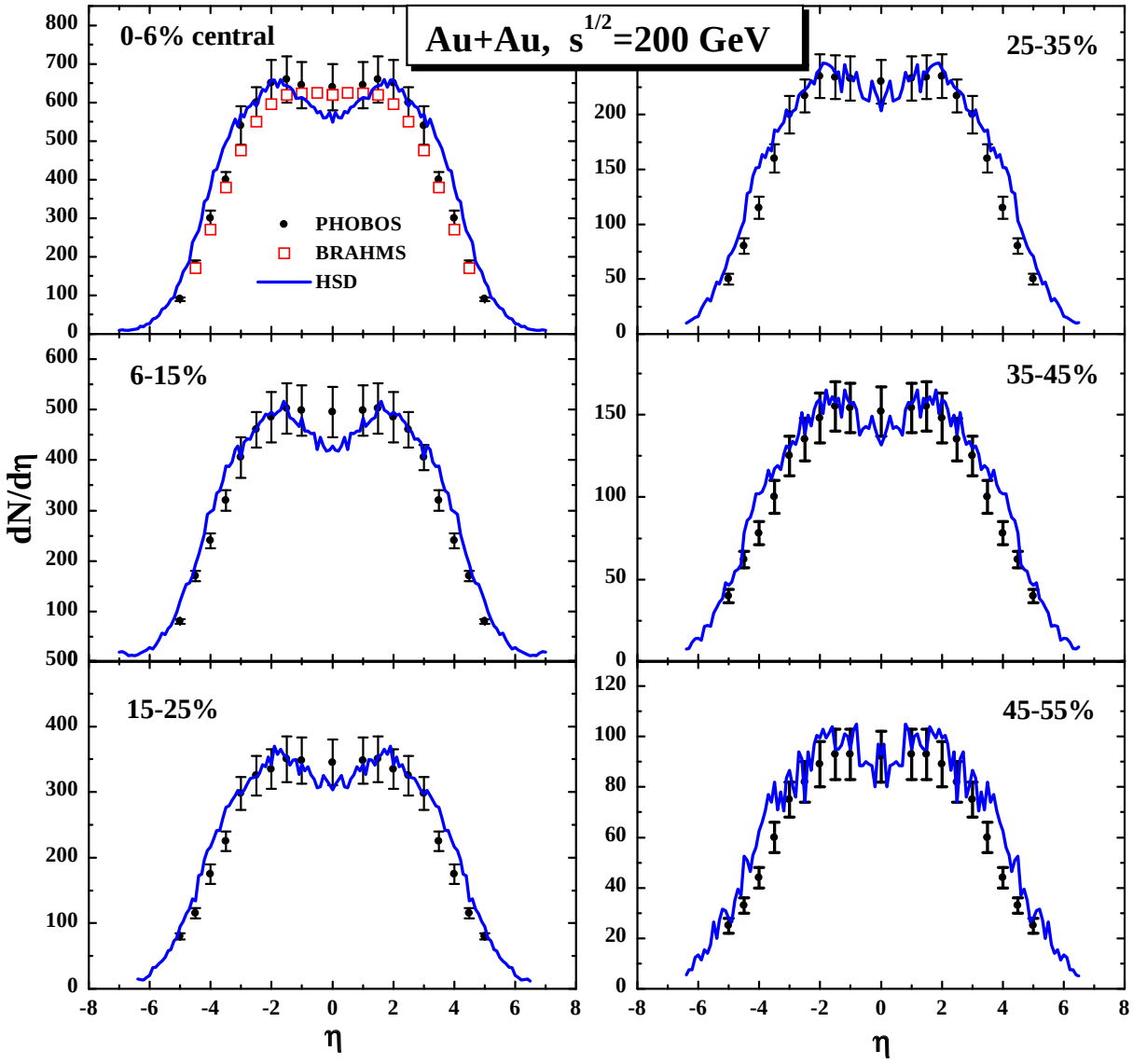

FIG. 1. The calculated pseudo-rapidity distributions of charged hadrons (solid lines) for $Au + Au$ at $\sqrt{s} = 200$ GeV for different centrality classes in comparison to the experimental data of the PHOBOS Collaboration [48] (full points), where the error bars indicate the systematic experimental uncertainty. The open squares in the upper left figure correspond to the data from the BRAHMS Collaboration for the same centrality class [49].

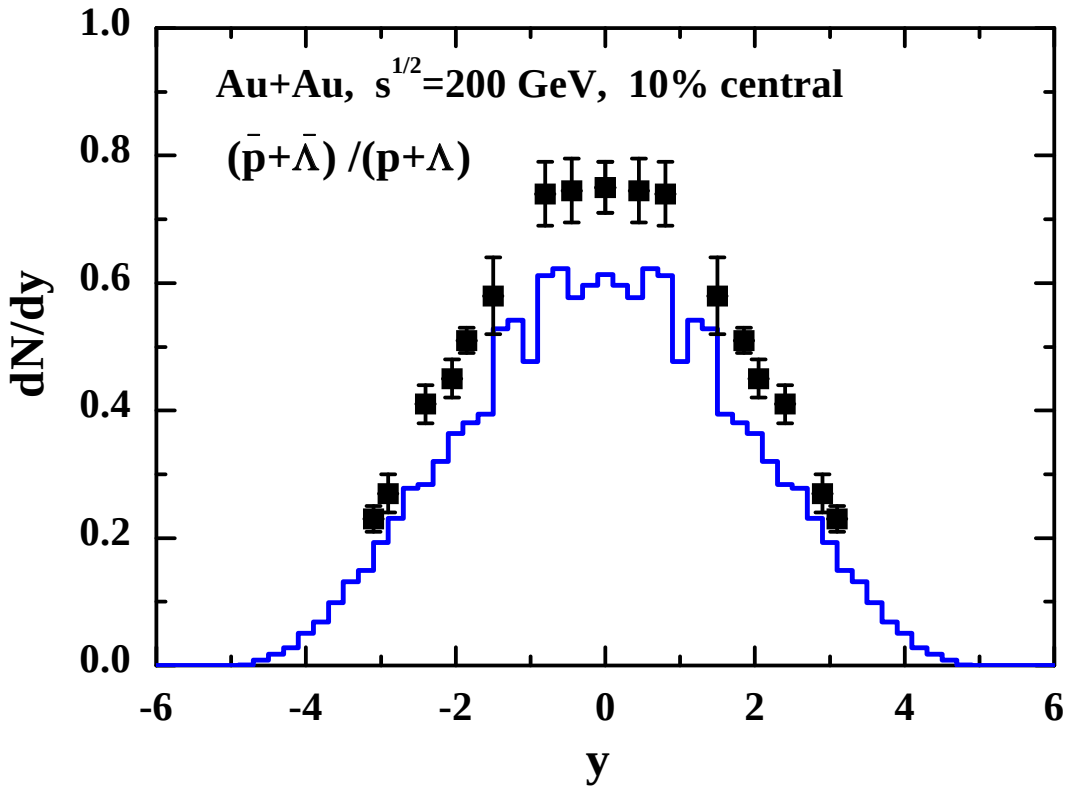

FIG. 2. The $(\bar{p}+\bar{\Lambda})/(p+\Lambda)$ ratio in 10% central $Au+Au$ collisions at $\sqrt{s}=200$ GeV as a function of rapidity y in comparison to the $\bar{p}/p$ data from the BRAHMS Collaboration [54]. Note, that the experimental data include some unknown fraction of Λ and $\bar{\Lambda}$ decays such that the comparison suffers from a 5-10% systematic uncertainty.

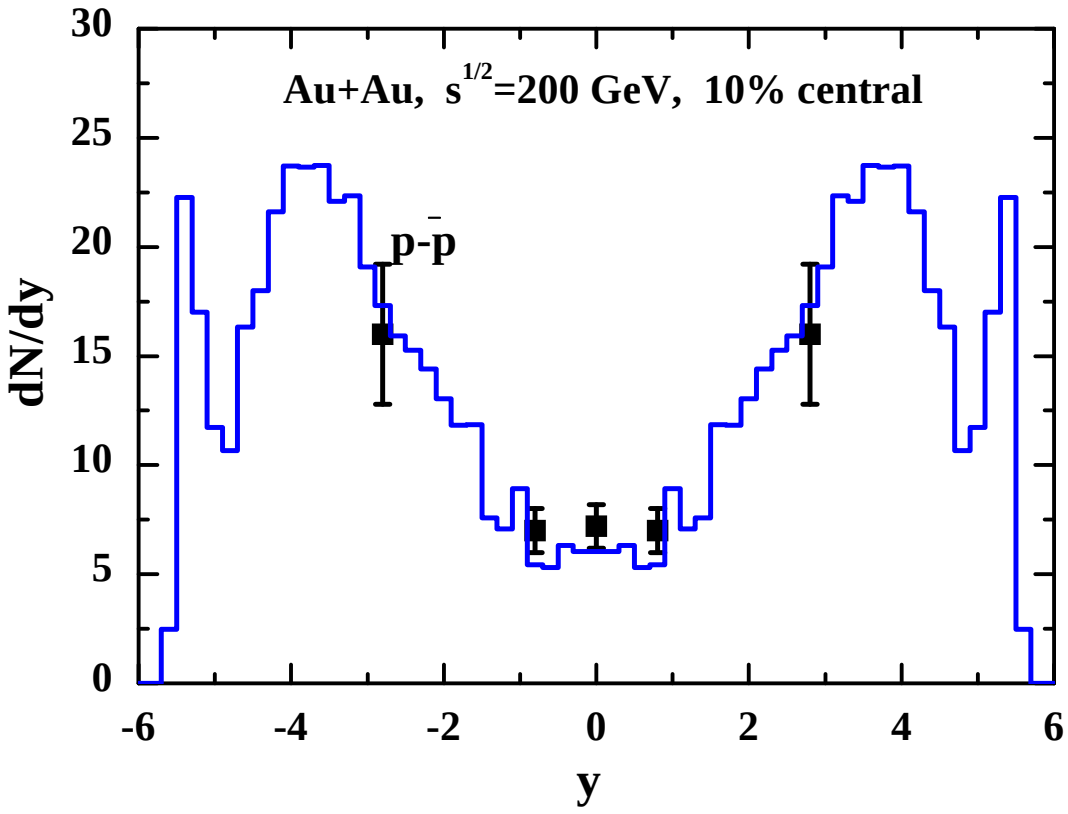

FIG. 3. The net proton $(p - \bar{p})$ rapidity distribution in central $Au + Au$ collisions at $\sqrt{s} =$ 200 GeV in comparison to the preliminary data of the BRAHMS Collaboration [55] for the same event class as in Fig. 2. Note, that the experimental data include some unknown fraction of Λ and $\bar{\Lambda}$ decays such that the 'real' $(p - \bar{p})$ rapidity distribution should be slightly lower.

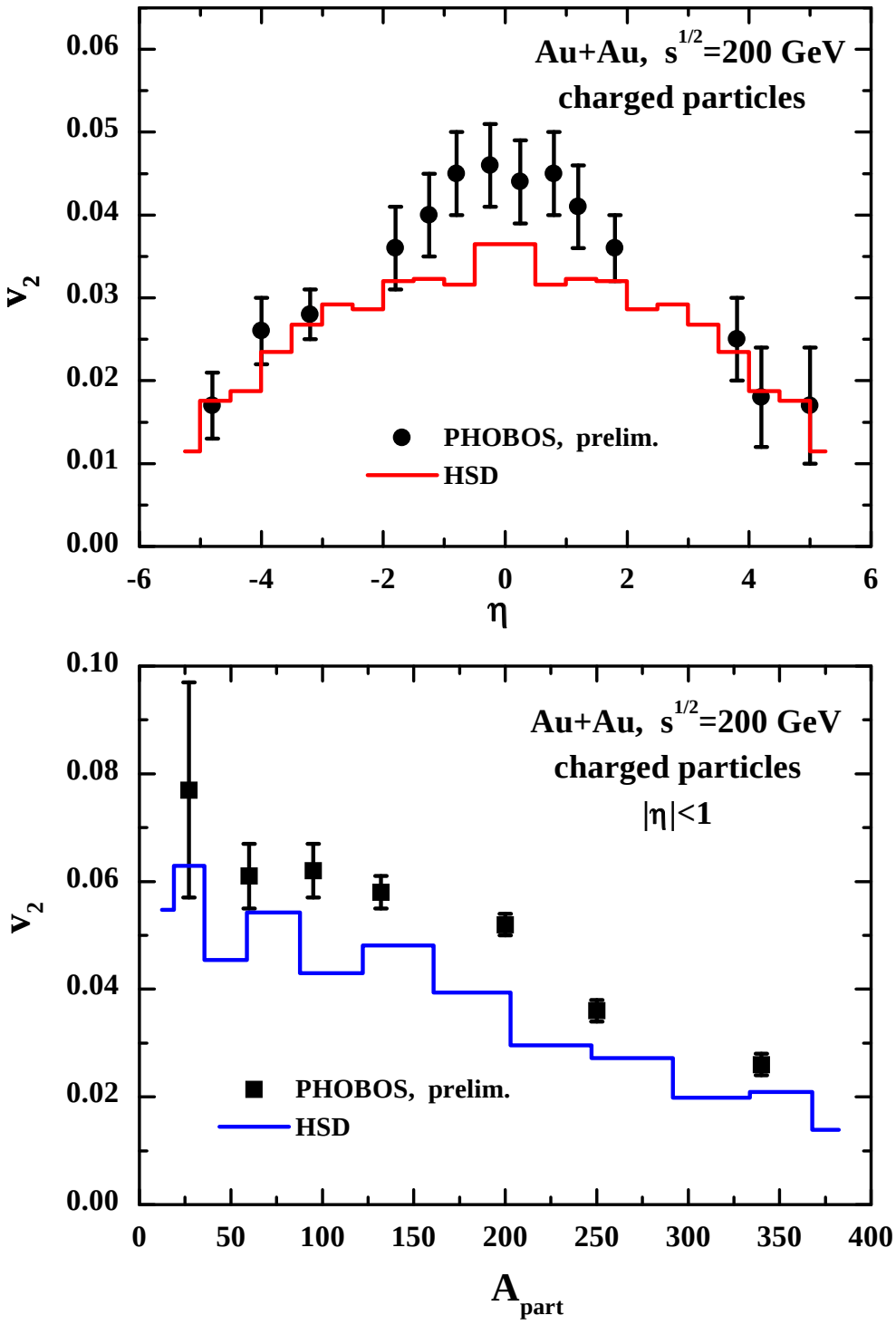

FIG. 4. The calculated elliptic flow v_2 for charged hadrons (solid lines) as a function of pseudorapidity η (upper part) and as a function of the number of 'participating nucleons' A_{part} for $|\eta| \leq 1$ (lower part) for $Au+Au$ collisions at $\sqrt{s} = 200$ GeV in comparison to the preliminary 'hit-based analysis' data of the PHOBOS Collaboration [58].

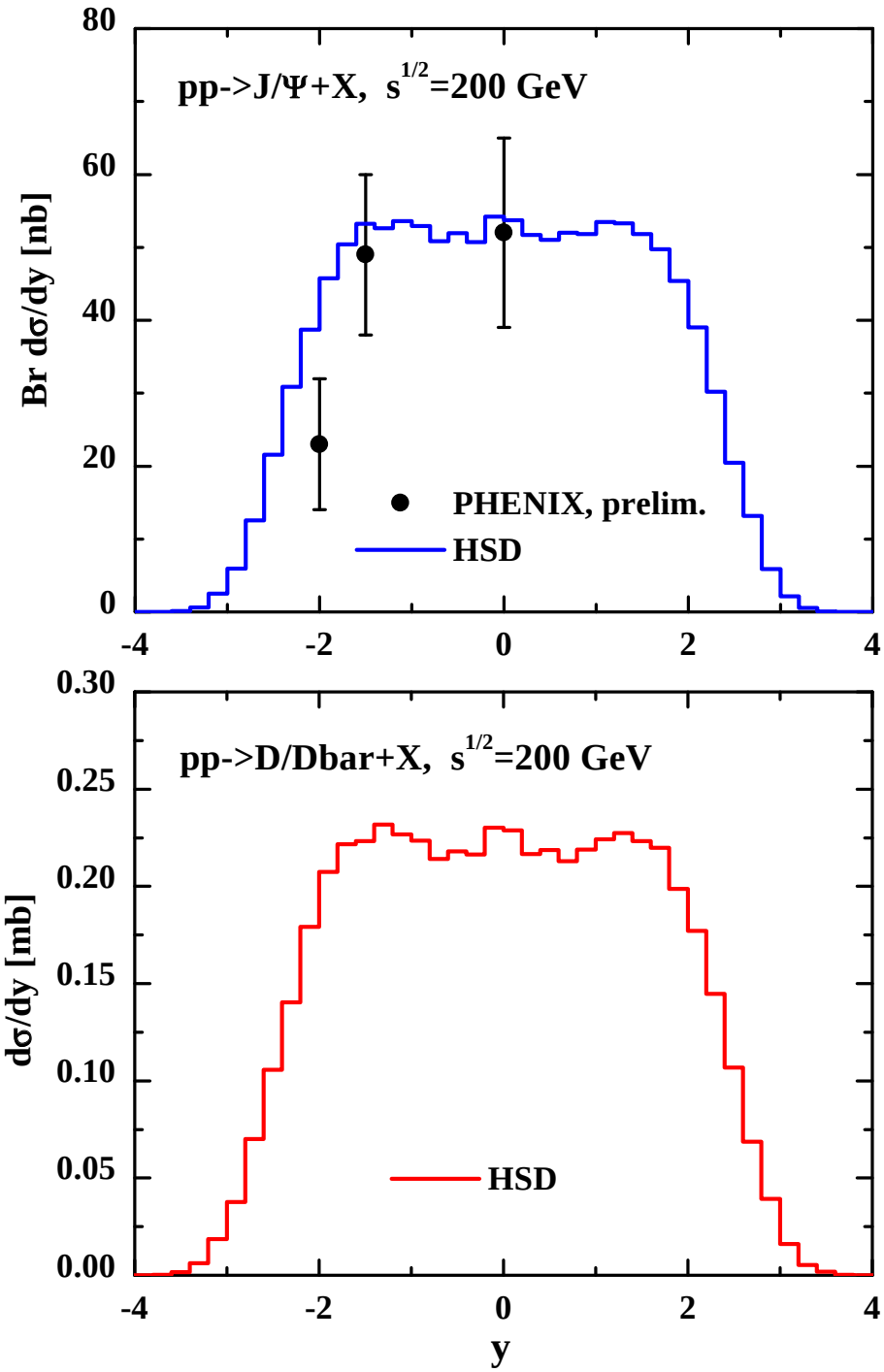

FIG. 5. The calculated rapidity distribution for J/Ψ mesons (upper part, multiplied by the branching to dileptons) and all open charm mesons (lower part) from pp collisions at $\sqrt{s} = 200$ GeV in comparison to the preliminary data from the PHENIX Collaboration [70] for $J/\Psi + X$. The $D + \bar{D}$ pair rapidity distribution is obtained by dividing the result in the lower part by a factor of ~ 2.

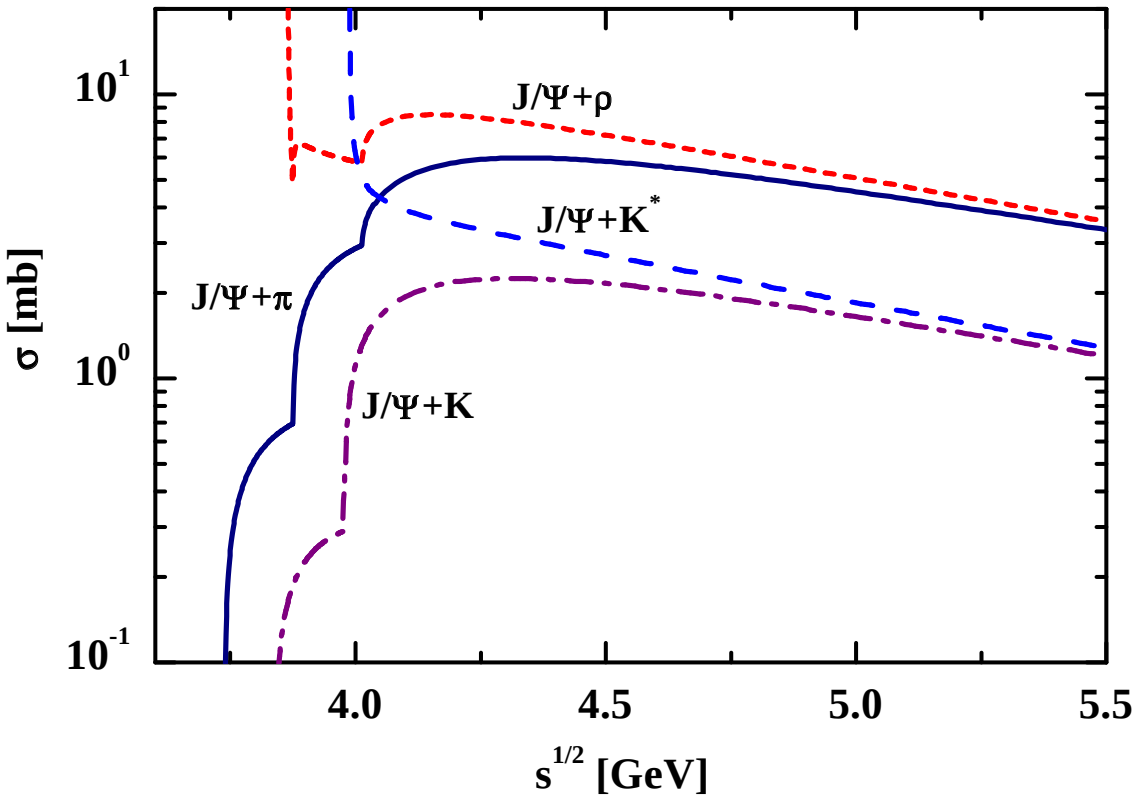

FIG. 6. The J/Ψ dissociation cross sections with π, ρ, K and K^* mesons as specified in Section 3.

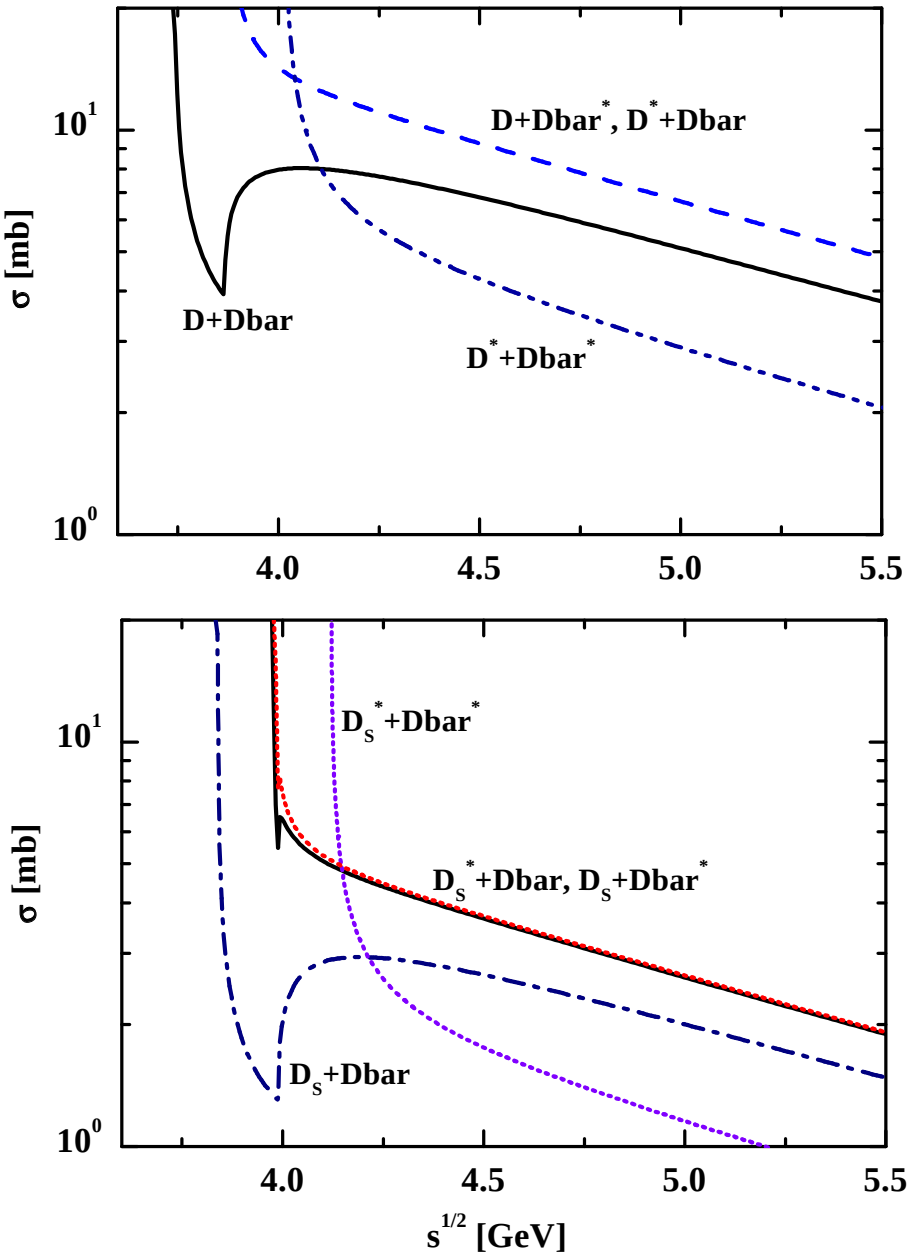

FIG. 7. The cross sections for the channels $D+\bar{D}, D+\bar{D}^*, D^*+\bar{D}, D^*+\bar{D}^* \to J/\Psi +$ meson (upper part) and the channels involving s or $\bar{s}$ quarks $D_s+\bar{D}$, $D_s+\bar{D}^*$, $D_s^*+\bar{D}$, $D_s^*+\bar{D}^+ \to J/\Psi+(K,K^*)$ (lower part) as a function of the invariant energy $\sqrt{s}$ according to the model described in Section 3.

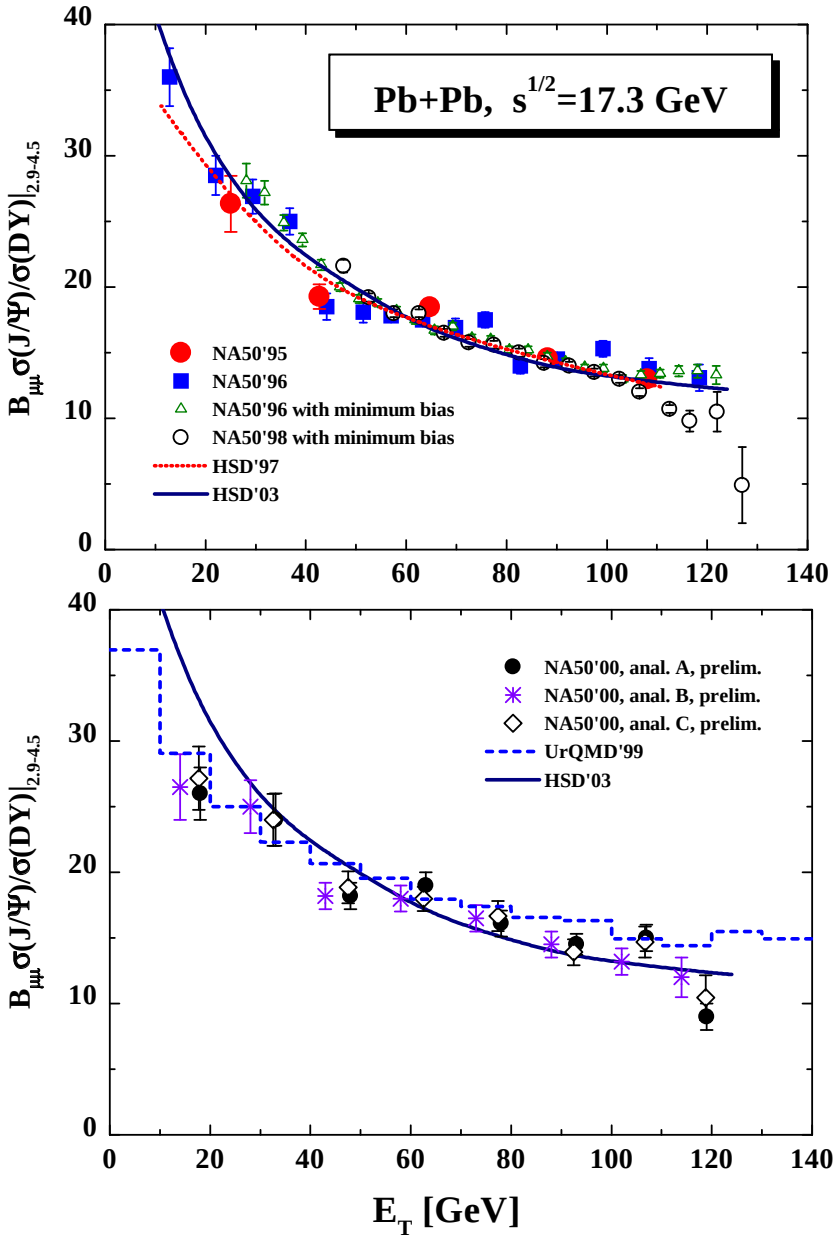

FIG. 8. The J/Ψ suppression (in terms of the $\mu^+\mu^-$ decay branch relative to the Drell-Yan background from 2.9 – 4.5 GeV invariant mass) as a function of the transverse energy E_T in $Pb + Pb$ collisions at 160 A GeV. The solid line (HSD'03) stands for the HSD result within the 'late' comover absorption scenario presented in Section 3 while the dotted line (HSD'97) reflects the earlier calculation from Ref. [81]. Upper part: the full dots stand for the NA50 data from 1995, the full squares for the 1996 data, the open triangles for the 1996 data with minimum bias while the open circles represent the 1998 data adopted from Refs. [7–10]. Lower part: the open and full symbols indicate the preliminary NA50 data from 2000 (analysis A, B and C) [11]. The dashed histogram is the UrQMD result from Ref. [18].

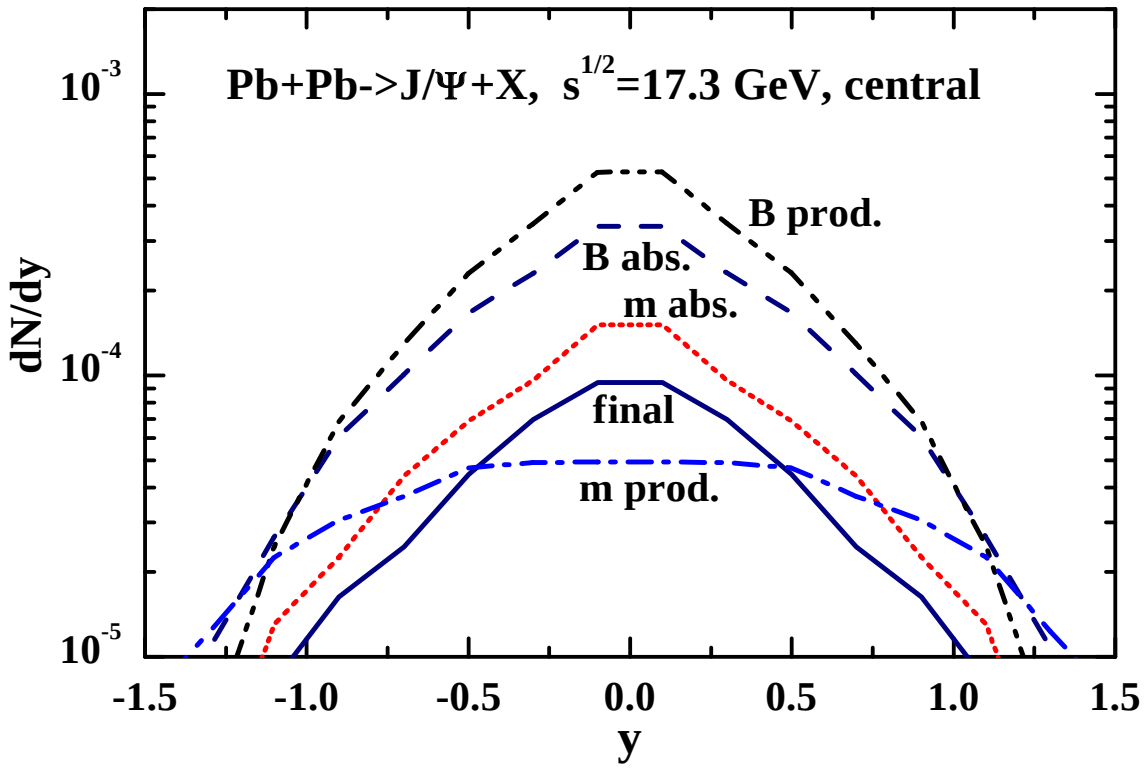

FIG. 9. Calculated J/Ψ rapidity distributions for central $Pb + Pb$ collisions at $\sqrt{s} = 17.3$ GeV. The ordering of the different lines is as follows: the upper dot-dot-dashed line stands for the rapidity distribution of J/Ψ mesons produced by initial BB collisions while the lowest dot-dashed line reflects the rapidity distribution of J/Ψ mesons from mB collisions. The dashed line corresponds to the J/Ψ's dissociated by baryons (B) and the dotted line shows the J/Ψ's dissociated by mesons (m). The full solid line gives the final J/Ψ rapidity distribution.

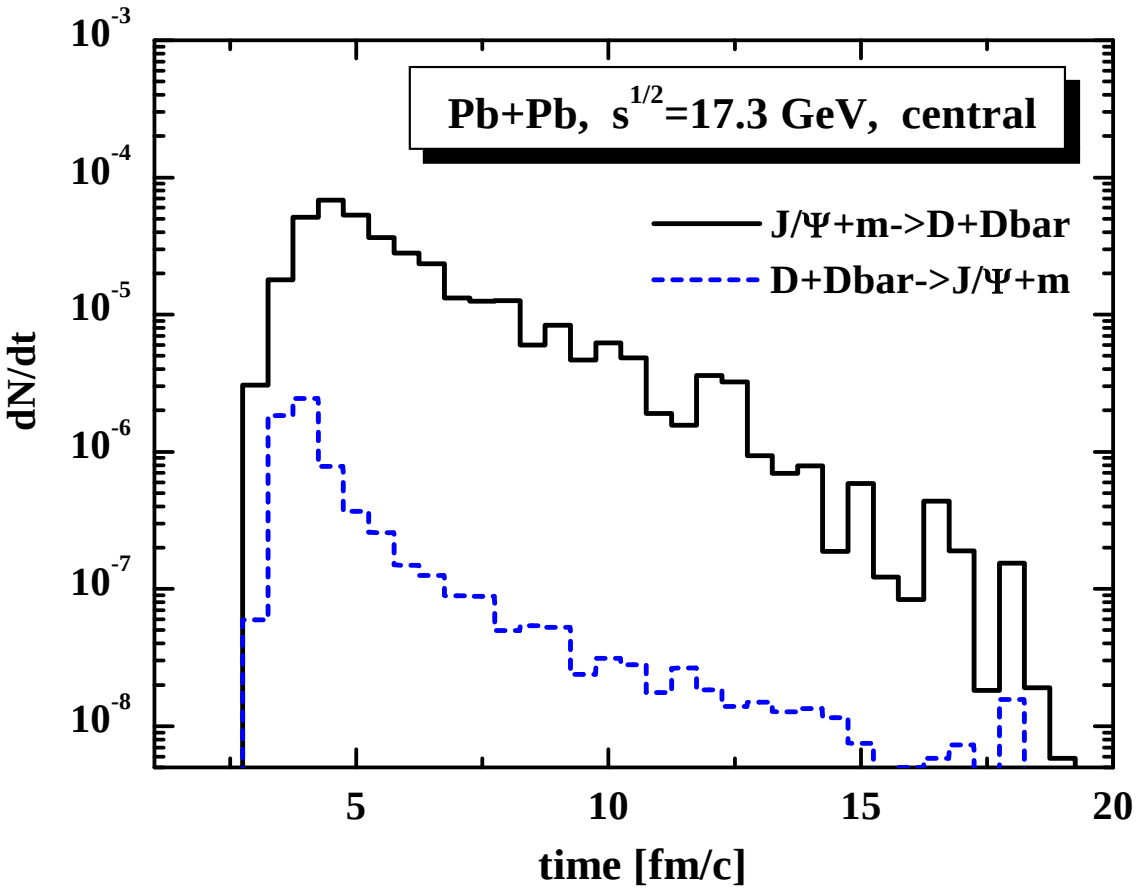

FIG. 10. The calculated rate of J/Ψ dissociation reactions with mesons (solid histogram) for central $Pb + Pb$ collisions at $\sqrt{s} = 17.3$ GeV in comparison the rate of backward reactions of open charm pairs to J/Ψ + meson (dashed histogram) according to the model specified in Section 3.

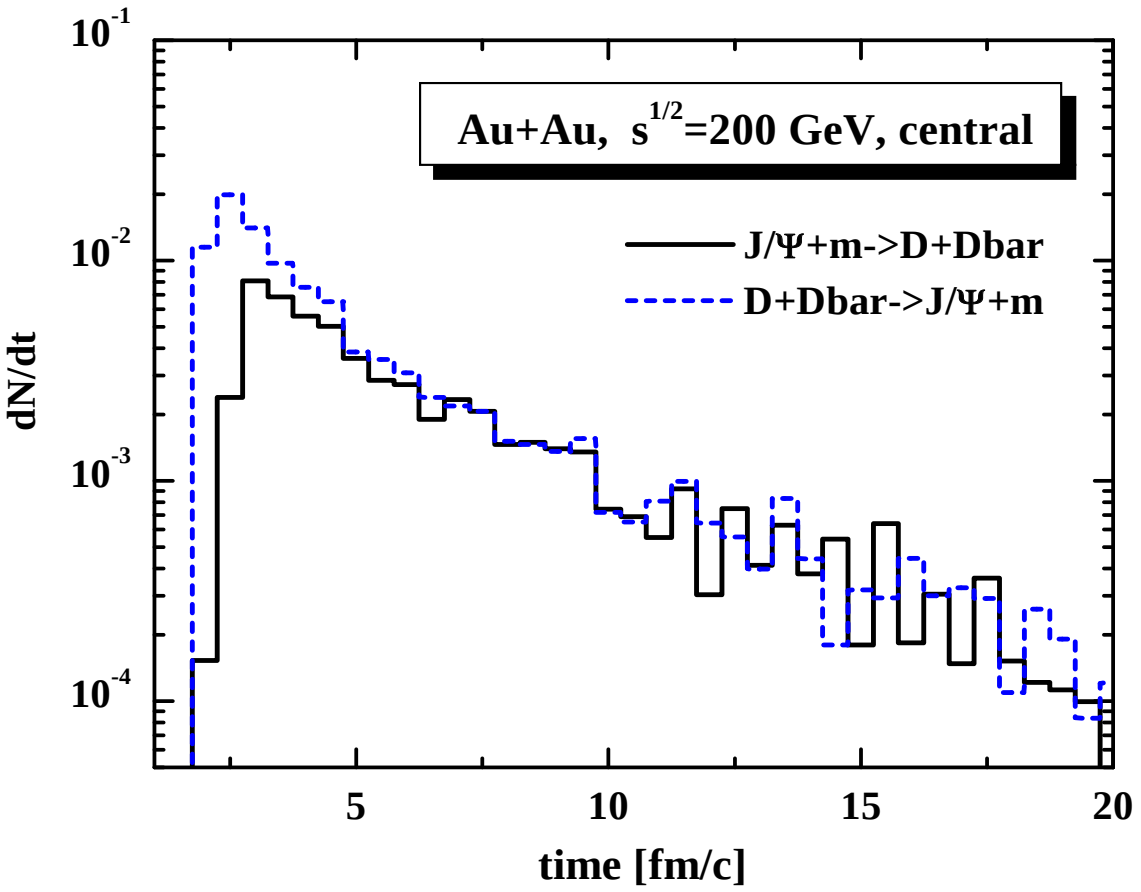

FIG. 11. The calculated rate of J/Ψ dissociation reactions with mesons (solid histogram) for central $Au + Au$ collisions at $\sqrt{s} = 200$ GeV in comparison the rate of backward reactions of open charm pairs to J/Ψ + meson (dashed histogram) according to the model specified in Section 3.

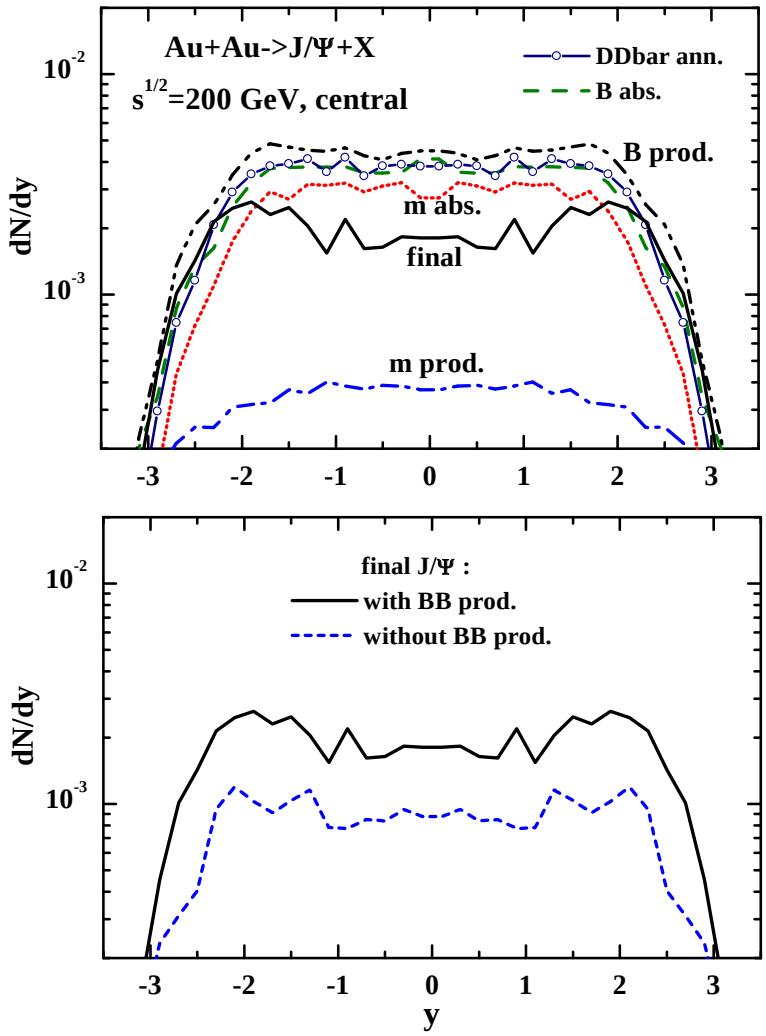

FIG. 12. Calculated J/Ψ rapidity distributions for 10% central $Au + Au$ collisions at $\sqrt{s}$ = 200 GeV. The ordering of the different lines in the upper part is as follows: the upper dot-dot-dashed line stands for the rapidity distribution of J/Ψ mesons produced by initial BB collisions while the lowest dot-dashed line reflects the rapidity distribution of J/Ψ mesons from mB collisions. The dashed line corresponds to the J/Ψ's dissociated by baryons (B); this distribution is approximately the same as the recreation of J/Ψ's from $D + \bar{D}$ annihilation (thin solid line with open circles). The dotted line ('m abs.') shows the J/Ψ's dissociated by mesons (m), which is slightly lower than the $D + \bar{D} \rightarrow J/\Psi$+meson recreation channel. The full solid line gives the final J/Ψ rapidity distribution. Lower part: The solid line is identical to the final J/Ψ rapidity distribution from the upper part whereas the dashed line is obtained from HSD calculations assuming that all charmonia produced from initial BB collisions are 'melted' in a possible QGP phase (see text).

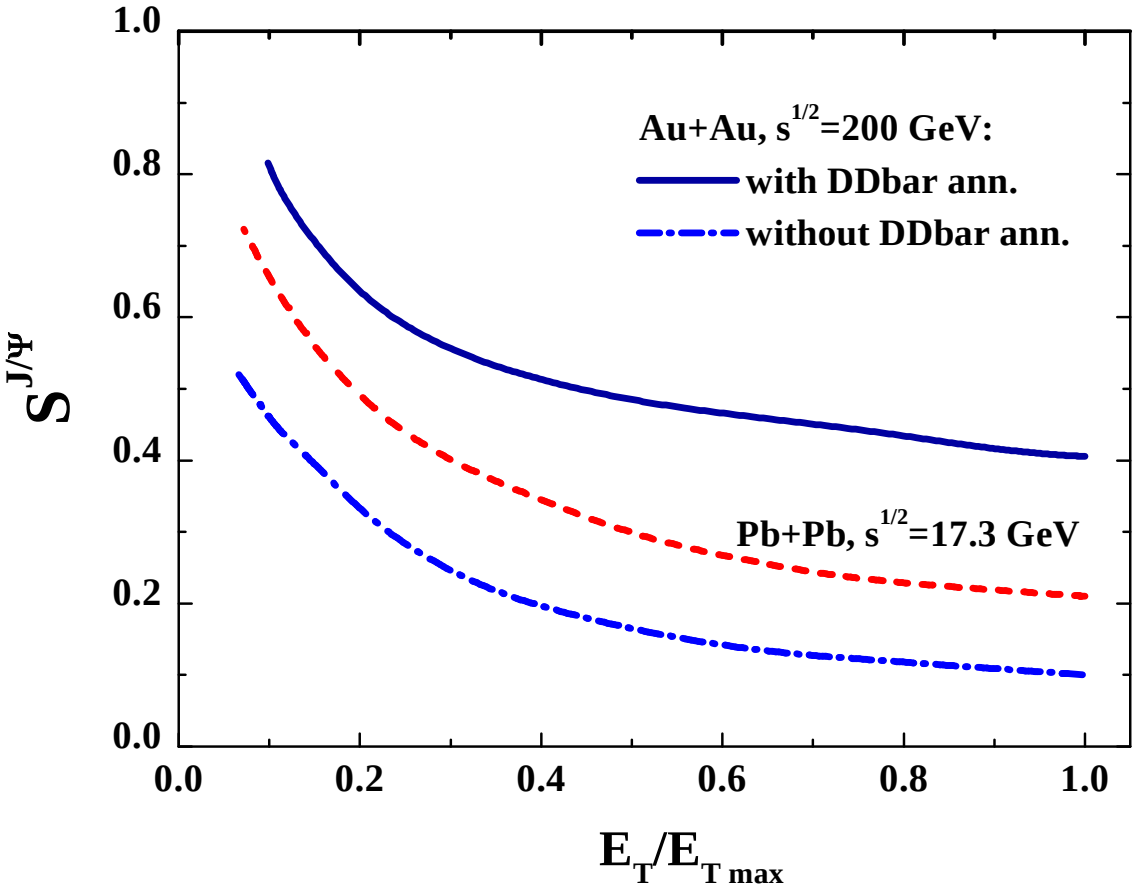

FIG. 13. The calculated J/Ψ survival probability $S_{J/\Psi}$ as a function of the transverse energy - in units of the transverse energy at impact parameter $b = 1$ fm – for $Au + Au$ collisions with (solid line) and without inclusion of the backward channels (lower dot-dashed line). The dashed line (middle) shows the result from Fig. 8 for the same quantity in $Pb + Pb$ collisions at $\sqrt{s} =$ 17.3 GeV for comparison.

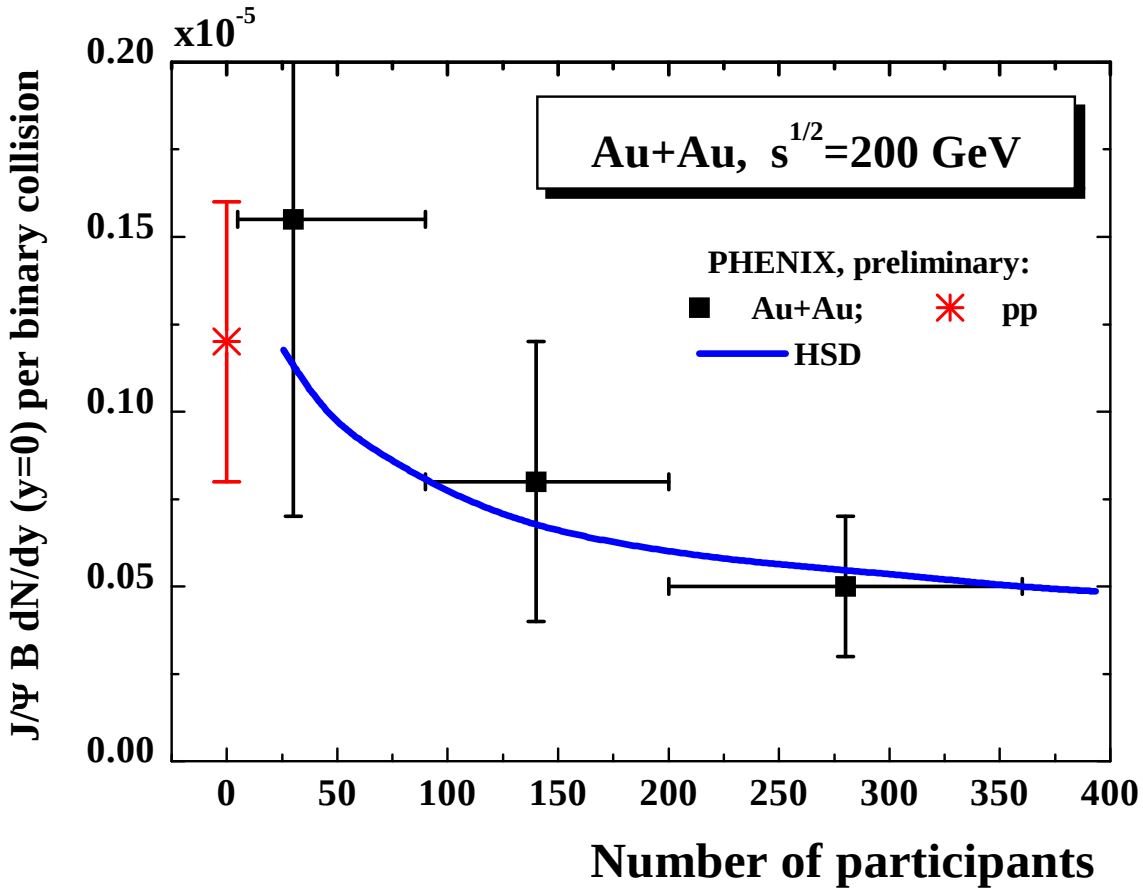

FIG. 14. The calculated J/Ψ multiplicity per binary collision – multiplied by the branching to dileptons – as a function of the number of participating nucleons N_{part} in comparison to the preliminary data from the PHENIX Collaboration [70] for $Au + Au$ and pp reactions.